

000 001 002 003 004 005 006 007 008 009 010 011 012 013 014 015 016 017 018 019 020 021 022 023 024 025 026 027 028 029 030 031 **CAED-Agent: AN AGENTIC FRAMEWORK TO AUTO-MATE SIMULATION-BASED EXPERIMENTAL DESIGN**

005 **Anonymous authors**
 006 Paper under double-blind review

009 ABSTRACT

012 The adjustment of parameters for expensive computer simulations is a challenging
 013 and universal task in the scientific research pipeline. We refer to these problems
 014 as **Cost-Aware Simulation-Based Experimental Design (CAED)**. Traditional ap-
 015 proaches include: a) brute force search, which is prohibitive for high-dimensional
 016 parameter combinations; b) Bayesian optimization, which struggles to generalize
 017 across setup variations and does not incorporate prior knowledge; c) case-by-case
 018 experts designs, which is effective but difficult to scale. Recent work on language
 019 models (LLMs) as scientific agents has shown an initial ability to combine pre-
 020 trained domain knowledge with tool calling, enabling workflow automation. Nat-
 021 urally, replacing the expert’s manual design with this automation seems to be a
 022 scalable remedy to general **CAED** problems. As will be shown in our empirical
 023 evaluations, LLMs lack cost awareness for parameter tuning tasks in scientific sim-
 024 ulation, leading to poor and inefficient choices. Inference-time scaling approaches
 025 enable better exploration, but the massive additional simulator queries they incur
 026 add up to total cost and contradict the target of being efficient. To address this
 027 challenge, we propose the **Cost-Aware Simulation-Based Experimental Design**
 028 Agent (**CAED-Agent**), an agentic framework that combines inference-time scal-
 029 ing with the cost-efficiency feedback from a lightweight surrogate model for solv-
 030 ing **CAED** problems. Our experiments in three different simulation cases show
 031 that **CAED-Agent** outperforms both Bayesian optimization and LLM baselines by
 032 significant margins, achieving success rates comparable to inference-time scaling
 033 with a ground truth simulator, while being far more cost-efficient.

034 1 INTRODUCTION

037 Simulation-based experimental design (Huan et al., 2024) involves tuning parameters for often ex-
 038 pensive simulators to achieve a specific design goal. A particular challenge in simulation-based ex-
 039 perimental design is to balance the outcome of interest (e.g., accuracy) versus the experimental costs:
 040 time, computational power, and financial budgets, aka **Cost-Aware Simulation-Based Experimental**
 041 **Design (CAED)**. Consider the design task in computational fluid dynamics (Anderson et al., 1995),
 042 where engineers need to juggle multiple design choices: low vs. high fidelity turbulence models,
 043 dimensionality reduction levels, spatial/temporal resolutions, and truncation limits for numerical
 044 solvers. Maximum-fidelity settings guarantee accuracy but can extend the runtime of simple sim-
 045 ulations from seconds to days, while overly coarse resolutions or model choices may fail to converge
 046 or yield unphysical solutions. Striking the correct balance in physical simulators is crucial for ac-
 047 complishing tasks within reasonable budgets.

048 Three common approaches address this challenge: 1) Brute force search, while comprehensive, be-
 049 comes prohibitive as parameter combinations grow exponentially. 2) Bayesian optimization (Snoek
 050 et al., 2012; Yao et al., 2024) and evolutionary algorithms (Perera et al., 2023) offer black-box alter-
 051 natives to grid search, but struggle to generalize across problem variations (e.g., laminar to turbulent
 052 flows, different geometry, or fluid to solid mechanics) and cannot leverage prior knowledge from
 053 related domains (Char et al., 2019; Trabucco et al., 2022). 3) Expert-based design, while most ef-
 054 fective for individual problems, is based heavily on human intervention and remains case-specific,
 055 limiting scalability in related problems (Fromer and Coley, 2024; Bharti et al., 2024).

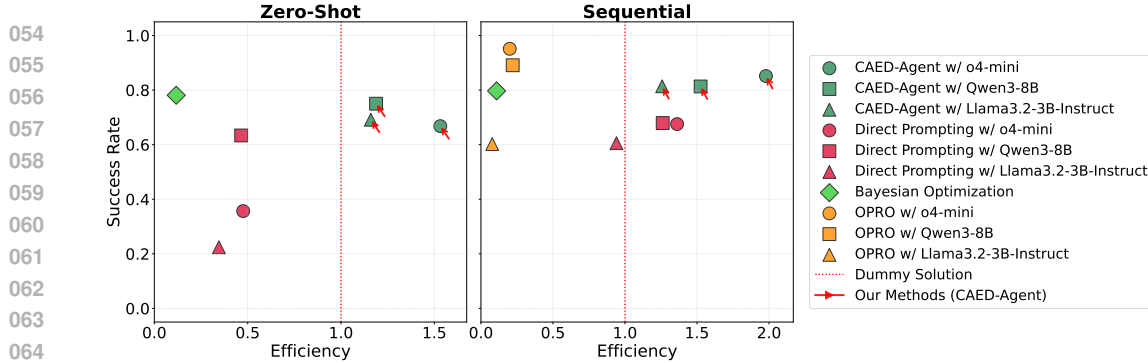


Figure 1: Performance averaged over simulators *Heat 1D*, *Euler 1D* and *NS Transient 2D*, in both Single-Turn setting (left) and Multi-Turn setting (right). *Efficiency* (\uparrow) is the mean normalized cost of the successful simulations; *Success Rate* (\uparrow) is the ratio of successful simulations. Compared to baselines OPRO (Optimization by PROMpting (Yang et al., 2023)) and BO (Bayesian Optimization with Gaussian Process (Nogueira, 2014)), our method achieves Pareto optima in all base models.

To address the scaling limitations of expert-based design, recent work explores large language models (LLMs) (OpenAI et al., 2024; Grattafiori et al., 2024; DeepSeek-AI et al., 2025) as tool-using agents (Ren et al., 2025) to conduct simulation-based experimental designs across domains (Zhong et al., 2024; Lv et al., 2025), potentially providing scalable expert-based intuitive design. These methods often require **inference-time scaling** to produce solutions on par with non-LLM methods. For example, BioDiscoveryAgent (Roohani et al., 2025) and LLAMBO (Liu et al., 2024) iteratively call tools multiple times, adding feedback to prompts for subsequent refinement. However, in real-world deployment, inference-time scaling’s computational cost becomes a critical limitation. Other works use token regression to predict experimental metrics (Chen et al., 2022; Song et al., 2024; Tang et al., 2025), such as cost awareness (Wu et al., 2024), for optimization. These works require extensive retraining of the model and tokenizer for specific tools, and assumes cost is a fixed tool property, which is invalid for physics-based simulations where cost depends heavily on parameter choices and simulation scenario setup.

In light of the computational overhead of inference-time scaling and training, some works use **neural-network** (NN) as surrogates for LLM directly calling the simulator (Lyu et al., 2024). However, neural surrogates are usually trained on a specific working condition and does not generalize to alternative settings. Moreover, as surrogates are direct maps from parameters to physical fields with no consideration of computation, they do not provide LLM agents with any insight on using the simulator efficiently. Combined, when encountering out-of-distribution (OOD) scenarios beyond the surrogate’s training range, agents must choose between inaccurate results predicted by the NN or calling the costly simulator, harming either the performance or the cost.

We propose training lightweight neural networks that learn only the low-dimensional cost-efficiency signal for cost-efficient inference-time scaling. The benefit is twofold: (1) data collection and model training are made easier as the simulation cost depends only on a few key numerical parameters such as spatial/temporal resolution and interpolation order; and (2) once the signal network is trained, it provides lightweight feedback within LLM inference-time scaling pipelines, enabling effective exploration scaling without expensive simulator evaluations. We call this methodology **Cost-Aware Simulation-Based Experimental Design Agent**. Our contributions are as follows.

1. We introduce **Cost-Aware Simulation-Based Experimental Design Agent**, a novel methodology that integrates a lightweight neural network that learns only the cost-efficiency feedback with LLM inference scaling frameworks for cost-aware simulation-based experimental optimization. To our knowledge, we are the first to combine low-dimensional cost-efficiency signal neural network with inference scaling for *CAED*.
2. We demonstrate in three physics simulator environments, each with varying environmental setting and precision requirements, that *CAED-Agent* significantly outperforms both traditional Bayesian optimization and state-of-the-art LLM-based approaches.
3. We provide a comprehensive benchmark for the design of simulation experiments based on cost-aware physics. Code for in-house simulator along with benchmark setups are open-sourced at [redacted].

108 **2 RELATED WORK**

110 **Non-LLM Methods for Experimental Design and Benchmarks.** Black-box optimization,
 111 particularly Bayesian approaches, represents a well-established experimental design frame-
 112 work (Smucker et al., 2018; Huan et al., 2024; Snoek et al., 2012; Knudsen et al., 2021; Pandita,
 113 2019), motivated by the complex procedures underlying experiments or simulators. Recent works
 114 explore state-of-the-art methods for experimental design and inverse problems, such as diffusion
 115 models (Daras et al., 2024). Benchmarks like Design-Bench (Trabucco et al., 2022) and Inverse-
 116 Bench (Zheng et al., 2025a) present 4-5 inverse design problems in scientific domains, respectively.
 117 However, few benchmarks or methods explicitly consider evaluation cost as an optimization target,
 118 making them unsuitable for our work. Consequently, we use in-house simulators for experiments.

119 **LLM for Experimental Design.** Recent work explores LLMs in agentic frameworks for scientific
 120 experimental design, using inference scaling to sample experimental trajectories. Examples include
 121 AI scientists autonomously designing experiments (Wang et al., 2023; Lu et al., 2024; Boiko et al.,
 122 2023), automated hypothesis generation frameworks (Zheng et al., 2025b; Wang et al., 2024), and
 123 LLM-driven laboratory automation (Bran et al., 2023; Jablonka et al., 2024). While demonstrating
 124 the potential of LLMs as experimental designers, these serve as “evidence papers” showing feasibil-
 125 ity rather than efficiency. Their pass@k metrics (k up to 256 or even 1024) are specially problematic
 126 for expensive experiments. MLEBench (Chan et al., 2025) represents a notable exception by incor-
 127 porating cost considerations (training time) for LLM on machine learning tasks, but does not capture
 128 the nuance of scientific experiment design. In contrast, we specifically target *CAED* as our research
 129 target, and contribute in-house simulator, evaluation, and benchmark setups.

130 **Large Language Models as Optimizers.** Recent studies leverage LLMs as black-box optimizers.
 131 OPRO (Yang et al., 2023) uses iterative LLM prompting while LLM-assisted EA (Hao et al., 2024)
 132 positions LLMs as evolutionary algorithm surrogates both requiring multiple evaluations per step.
 133 Other approaches (Song et al., 2024; Chen et al., 2022; Liu et al., 2024; Tang et al., 2025) similarly
 134 depend on extensive evaluations for inference or post-training data generation. Their fundamental
 135 limitation is expensive trajectory generation requiring abundant simulator queries, computationally
 136 infeasible for costly experiments. Our method combines inference scaling with lightweight signal
 137 neural network for efficient cost-aware trajectory generation, avoiding expensive simulator queries.

138 **3 METHODOLOGY**

139 **3.1 PROBLEM DEFINITION**

140 Given design variable space \mathcal{X} (e.g., spatial/temporal resolution, spatial interpolation methods), en-
 141 vironmental parameter space Θ (e.g., initial or boundary conditions), and output observation space
 142 \mathcal{Y} , we define the forward simulation-based experimental process as $\mathcal{F} : \mathcal{X} \times \Theta \rightarrow \mathcal{Y}$:

$$y = \mathcal{F}(x, \theta), \quad \text{where } x \in \mathcal{X}, \theta \in \Theta \quad (1)$$

143 With utility function $\Phi : \mathcal{Y} \times \Theta \rightarrow \mathbb{R}$ (e.g. representing accuracy or physical validity of simulated
 144 results) and cost function $\mathbf{C} : \mathcal{X} \times \mathcal{Y} \times \Theta \rightarrow \mathbb{R}$ (e.g. wall time, complexity analysis, RAM
 145 consumption), the *CAED* problem becomes:

$$x^* = \arg \max_{x \in \mathcal{X}} (\Phi(y, \theta), -\mathbf{C}(x, y, \theta)) \quad (2)$$

146 In this work, we define computational cost as the number of floating point operations (consistent
 147 with complexity analysis) and normalize cost relative to a brute-force reference (dummy) solution
 148 z_θ that satisfies accuracy requirements with optimal cost (within a coarse search granularity):

$$\hat{\mathbf{C}}(x, y, \theta) = \frac{\mathbf{C}(x, y, \theta)}{\mathbf{C}(z_\theta, \theta)}. \quad (3)$$

149 Following previous works (Snoek et al., 2012; Fromer and Coley, 2024), we combine the normalized
 150 cost and utility objectives into a single reward metric for an experiment (x, y, θ) :

$$\mathcal{R}^0(x, y, \theta) = \frac{\Phi(y, \theta)}{\hat{\mathbf{C}}(x, y, \theta)} \quad (4)$$

We consider two variants of the *CAED* problem: Single-Turn *CAED*, where the algorithm proposes only one configuration, and Multi-Turn *CAED*, where the algorithm proposes a trajectory of configurations for iterative refinement (Huan et al., 2024; Bharti et al., 2024)):

Definition 3.1 (Single-Turn Cost-Aware Simulation-Based Experimental Design (*CAED*)).

$$\mathcal{Q}_0 : x^* = \arg \max_{x \in \mathcal{X}} \mathcal{R}^0(x, y, \theta), \quad (5)$$

Definition 3.2 (Multi-Turn Cost-Aware Simulation-Based Experimental Design (*CAED*)).

$$\mathcal{Q}_m : \{x\}^* = \arg \max_{\{x_1, \dots, x_n\} \in \mathcal{X}^*} \mathcal{R}^s(\{x_1, \dots, x_n\}, \{y_1, \dots, y_n\}, \theta), \quad (6)$$

where \mathcal{X}^* is a sequence consisting of an arbitrary number of elements from \mathcal{X} . In this work, we allow multi-turn solutions with any length. $\{y\} = \{y_1, y_2, \dots, y_n\}$ are observations from sequence $\{x\} = \{x_1, x_2, \dots, x_n\}$, and the modified multi-turn reward \mathcal{R}^m is:

$$\mathcal{R}^m(\{x_1, \dots, x_n\}, \{y_1, \dots, y_n\}, \theta) = \frac{\max_i \Phi(y_i, \theta)}{\sum_i \hat{\mathbf{C}}(x_i, y_i, \theta)}, \quad (7)$$

i.e., the ratio between maximum utility and total cost incurred by this sequence of proposals.

The two variants of the *CAED* problem, \mathcal{Q}_0 and \mathcal{Q}_m , are distinct and have different metrics with different reference solution z_θ . They evaluate different abilities of the solution: \mathcal{Q}_0 requires an intuitive choice of simulation parameter, while \mathcal{Q}_m requires adaptation based on simulation feedback. They are not to be recognized as the same task with a varying hyperparameter (number of turns).

3.2 COST-AWARE SIMULATION-BASED EXPERIMENTAL DESIGN AGENT

Overview. We adopt the inference-time scaling framework of Optimization by PROmpting (OPRO) (Yang et al., 2023; Song et al., 2024; Chen et al., 2022), with the addition of a module that efficiently provides utility $\Phi(x, y, \theta)$ and cost $\hat{\mathbf{C}}(x, y, \theta)$ information without calling the expensive ground-truth simulations. Specifically, we train a neural-network surrogate to predict these scalar signals from the design variables and environmental parameters. Because the scalar outputs are strongly correlated with a few key design variables, signal model training converges with fewer samples and smaller model size, compared with full-physics surrogates (Ghafariasl et al., 2024; Hou and Evins, 2024); see C for details. The signal model then supplies feedback, the predicted utility and cost, to the LLMs proposed parameter designs. These feedback signals, recorded as designvalue pairs, are appended to the prompts history as in-context examples to aid the LLMs optimization output. See Figure 2 for an illustration of *CAED-Agents* workflow.

Signal Neural Network. We train lightweight networks $\mathcal{S} : \mathcal{X} \times \Theta \rightarrow \mathbf{D}_\Phi \times \mathbb{R}$ to predict utility and cost signals only, where \mathbf{D}_Φ is the short-hand for the range of utility function Φ . Our experiments show that small fully connected neural networks can learn the function well for the experiments in this paper, though we note that architecture and model size can be adapted according to the need of specific solvers. See Appendix C for details on neural network implementation for this paper.

To provide rich, informative utility signals, as opposed to the binary boolean signals in prior works (Smucker et al., 2018; Huan et al., 2024), we design a reward shaping function f that maps the binary experiment outcome $b(y) \in \{0, 1\}$ to a scalar soft success measure $f(y) \in [0, 1]$ defined as follows.

Definition 3.3 (Soft Utility Function). Following the notations in section 3.1, let \mathcal{Y} be the experiment’s observation space, Θ be the environmental variable space, and Φ be the original utility function. Define the feasible set

$$\mathcal{G}_\theta := \{y \in \mathcal{Y} : \Phi(y, \theta) = 1\}. \quad (8)$$

We call a mapping $f : \mathcal{Y} \times \Theta \rightarrow [0, 1]$ a *soft utility function* if it satisfies:

- (i) Feasibility calibration: $\forall y \in \mathcal{G}_\theta : f(y) = 1, \sup_{y \notin \mathcal{G}_\theta} f(y) < 1$.
- (ii) Normalization: $0 \leq f(y) \leq 1, \forall y \in \mathcal{Y}$.
- (iii) Monotone alignment: $\Phi(y_1) \preceq \Phi(y_2) \implies f(y_1) \leq f(y_2)$.

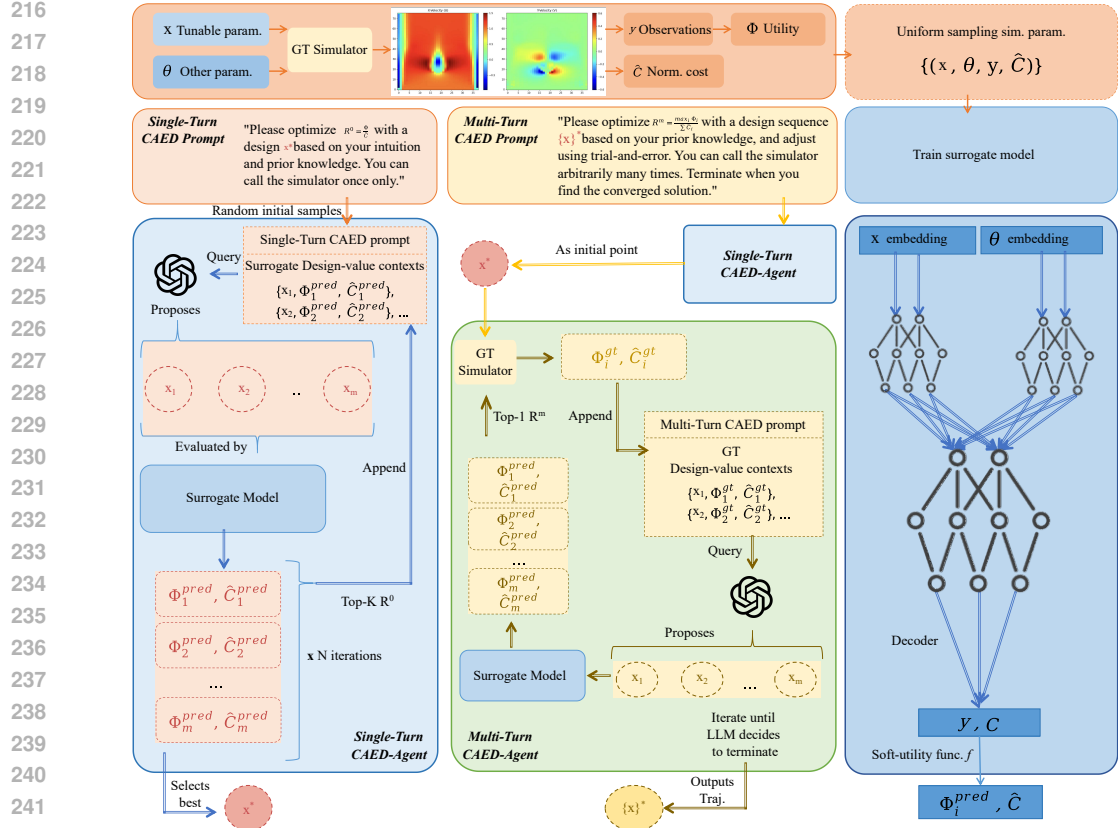


Figure 2: Overview of CAED-Agent. For a given simulation-based experimental design problem, CAED-Agent samples uniformly within design space to train a neural network surrogate for feedback signals of utility and cost (right). In the Single-Turn CAED setting (left), the LLM agent proposes an ensemble of candidate designs, calls the simulator to obtain feedback, and extend the design-score pairs history for the next iteration of candidate ensemble generation. Finally the LLM selects the best design at the last iteration based on surrogate signals. In the multi-turn CAED setting (middle), the LLM sends the best design based on surrogate signal for actual evaluation at each decision step, receives actual evaluation feedback alongside surrogate signals, and output the trajectories of designs sent for ground-truth evaluation as solution.

The signal neural network \mathcal{S} learns the soft utility signal $f(y)$ in the place of $\Phi(y)$. We provide the following proposition that any soft utility function f guarantees an incremental performance over binary utility functions when integrated into our framework, and a well-designed f will lead to more significant improvements. Refer to Appendix D for our design of f and proofs of the proposition.

Definition 3.4 (Policies). Recall that $R^0(x, y, \theta)$ and $\mathcal{R}^m(\{x_1, \dots, x_n\}, \{y_1, \dots, y_n\}, \theta)$ are respectively single-turn and multi-turn reward defined in Eq.1). For a task instance θ , we define two policies:

- (i) **Binary-utility policy** $\pi_{\text{bin}}(x_t \mid \theta, h_{t-1})$: at step t , given history $h_{t-1} = \{(x_s, y_s, b(y_s, \theta))\}_{s=1}^{t-1}$, sample the next design x_t ; denote the induced distribution over the final design by $x \sim \pi_{\text{bin}}(\cdot \mid \theta)$.
- (ii) **Soft-utility policy** $\pi_f(x_t \mid \theta, h_{t-1})$: replace b with any soft utility f from Definition 3.3, i.e., the history stores $(x_s, y_s, f(y_s, \theta))$. Denote the resulting final-design distribution by $x \sim \pi_f(\cdot \mid \theta)$.

Proposition 3.5 (Soft utility dominates binary utility in expected reward). *Fix a base model and any soft utility f in Definition 3.3, the expected reward under the soft-utility policy is no worse than under the binary-utility policy:*

$$\mathbb{E}_\theta \mathbb{E}_{x \sim \pi_f^0(\cdot \mid \theta)} [R^0(x, \theta)] \geq \mathbb{E}_\theta \mathbb{E}_{x \sim \pi_{\text{bin}}^0(\cdot \mid \theta)} [R^0(x, \theta)].$$

$$270 \quad \mathbb{E}_\theta \mathbb{E}_{\{x\} \sim \pi_f^m(\cdot|\theta)} [R^m(\{x\}, \theta)] \geq \mathbb{E}_\theta \mathbb{E}_{\{x\} \sim \pi_{\text{bin}}^m(\cdot|\theta)} [R^m(\{x\}, \theta)]. \\ 271$$

272 In summary, for a given simulation-based experimental design task, we train a lightweight network
 273 $\mathcal{S} : \mathcal{X} \times \Theta \rightarrow \mathbf{D}_\Phi \times \mathbb{R}$ to predict a certain design’s utility and cost; in cases where utility function
 274 Φ is sparse and less informative, we substitute it with soft utility function f and learn soft utility
 275 signals, i.e. we learn $\mathcal{S} : \mathcal{X} \times \Theta \rightarrow \mathbf{D}_y \times \hat{\mathbf{C}}$, where \mathbf{D}_y is the range of f . The trained network \mathcal{S}
 276 provides feedback for the following agent’s self-refinement.

277 **Agentic Framework.** The agent leverages Optimization by PROmpting (OPRO) as the base LLM
 278 in-context optimization method, and use the signal network’s feedback as in-context examples. We
 279 note that expanding to other inference-time scaling methods is straightforward and requires no
 280 change or re-training of the signal neural network. Pseudocode for our agent implementation is
 281 provided in Appendix B.
 282

283 For Single-Turn *CAED*, the agent starts with 5 (a hyper-parameter to adjust based on inference budget)
 284 uniformly-sampled tuples of (design variable, utility, efficiency) evaluated by surrogate neural
 285 network. Then the agent iteratively proposes ensembles of candidate design choices, receives neural
 286 network feedback for the entire ensemble, and append them to the example pool. The example pool
 287 is managed as a priority queue with key (utility, efficiency) and presented to the model in ascending
 288 order. The example pool only keeps top-10 samples (also a hyper-parameter) to concise the context.
 289 The process is repeated for a fixed number of iterations, and the best design in the example pool is
 290 chosen for the final design. The fixed number of iterations is another hyperparameter reflecting the
 291 allowed LLM inference budget.

292 To solve Multi-Turn *CAED*, we warm-start with Single-Turn *CAED* solution for the first round of
 293 ground truth simulator evaluation, and then append the results to the pool. This process is repeated
 294 for each iteration to find the most promising proposals for simulator evaluation. In short, the Single-
 295 Turn *CAED* works as an acquisition function for each of the multi-turn steps. The loop terminates
 296 when either the LLM decides that a satisfactory solution is found or the computation cap is reached.
 297

298 4 EXPERIMENTS

300 4.1 EXPERIMENTAL ENVIRONMENT

301 We demonstrate the ability of *CAED-Agent* on three physics simulators: (1) 1D heat conduction
 302 equation with mixed boundary conditions, (2) 1D compressible inviscid flow with Euler equation,
 303 and (3) 2D transient incompressible Navier–Stokes equation, referred to as *Heat 1D*, *Euler 1D* and
 304 *NS Transient 2D* respectively, for brevity. Appendix A contains details on the design variable space
 305 \mathcal{X} , observation space \mathcal{Y} , and parameter space Θ . We focus on spatial resolution tuning tasks, where
 306 the tunable parameter governs the spatial resolution of the simulation, creating a trade-off between
 307 simulation accuracy and computational cost. The tunable parameters in our experiments are:

- 308 1. The number of grid numbers (n_space) for *Heat 1D* and *Euler 1D*
- 309 2. The grid resolution along X-axis (*resolution*) for *NS Transient 2D*

310 We design three precision level goals δ for each task, reflecting moderate to stringent accuracy
 311 requirements in real-world experiments. For each task and each precision level, we evaluate the
 312 methods on around 25 settings varying in environmental parameters.

313 For each problem instance characterized by θ , we first obtain a (near-)optimal design z_θ via brute-
 314 force search that guarantees successful convergence, e.g. through iteratively doubling the parameter
 315 until successful, serving as a reference point for both accuracy and cost. This is solely for the
 316 evaluation of our method and not necessary in practice. We then define the success of the simulation
 317 through the following utility function:
 318

$$319 \quad \Phi(\mathcal{F}(x, \theta), \theta) = \mathbf{1}\{ \|\mathcal{F}(x, \theta) - \mathcal{F}(z_\theta, \theta)\|_2 \leq \delta \}, \quad (9)$$

320 Where $\mathbf{1}$ is the indicator function, $\|\cdot\|_2$ is the root mean square error across dimensions of the
 321 observation space, and δ is a tolerance parameter reflecting various precision needs in real-world
 322 applications. The success rate is defined as the ratio of successful simulations where $\Phi(\mathcal{F}(x, \theta)) = 1$.
 323 The cost \mathbf{C} is defined as previously introduced in our problem formulation.

324 **4.2 BASELINES AND SETTING**
 325

326 We compare our results against the following baselines. **Bayesian Optimization (BO)**: We use a
 327 classic implementation (Nogueira, 2014) with Gaussian Process (GP) (Rasmussen, 2004) and Upper
 328 Confidence Bound (UCB) (Berk et al., 2020). We used consistent training samples for the signal
 329 neural network *CAED-Agent* and for the GP regressor to achieve a fair comparison. **Direct query**
 330 to **LLM medels** (*Direct Query*) and the original **Optimization by Prompting (OPRO)** (Yang et al.,
 331 2023) are LLM-based approaches. For all LLM-based methods (including our *CAED-Agent*), we
 332 design a shared set of prompts explaining the Physics scenario, optimization target and simulator
 333 calling APIs; refer to E for examples. Notably, *OPRO* requires repeated evaluations of the ground-
 334 truth simulator; therefore, we restrict its use to the Multi-Turn setting.
 335

336 For the implementation of *CAED-Agent*, we trained a lightweight neural network for each task
 337 (*Heat 1D*, *Euler 1D*, and *NS Transient 2D*) separately, each with approximately 10k parameters
 338 and trained on about 4k sampled points per problem. The networks outputs are the RMSE to the
 339 reference solution and the cost. At inference time, we map the predicted RMSE to a utility signal
 340 using the soft utility functions described in Definition 3.3; we also compare using the binary utility
 341 Φ in ablation studies. See Appendix C for details.
 342

343 **4.3 METRICS**
 344

345 For ease of future reference, we denote the optimization targets in 5 and 6 as respectively R^0 and
 346 R^m , referring to them as Single-Turn or Multi-Turn *Reward Functions*. We also report success rates
 347 P^0 and P^m to help us better understand the qualities of proposed solutions.
 348

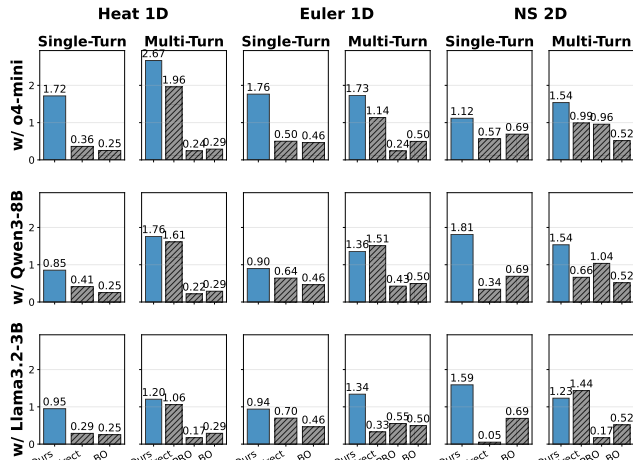
$$R^0 = \frac{\Phi(\mathcal{F}(x, \theta), \theta)}{\hat{\mathbf{C}}(x, \theta)}, \quad R^m = \frac{\max_i \Phi(\mathcal{F}(x_i, \theta), \theta)}{\sum_i \hat{\mathbf{C}}(x_i, \theta)}$$

349 **4.4 ANALYSIS**
 350

351 We refer readers to Table 2 of F for complete results in three scenarios; here we report the following
 352 findings that help understand and verify the efficacy of our method.
 353

354 **Our method outperforms most**
 355 **baselines in terms of R^0 and R^m .**
 356 As shown in Figure 3 and Figure 1,
 357 our method outperforms all comparisons in the Single-Turn setting and
 358 all but a few exceptions in the Multi-Turn setting. We argue that these sub-
 359 optimal cases are due to the inferior reasoning ability of open-source mod-
 360 els, causing them to occasionally fail to refine their solutions based on feed-
 361 back. Note that in many cases, es-
 362 pecially in the easier scenarios *Heat*
 363 and *Euler 1D*, OPRO and BO are
 364 significantly worse than Direct Query,
 365 whereas our method is significantly
 366 better. This is because convergence
 367 is relatively easy in such scenarios, so
 368 the additional ground-truth simulator
 369 calls used by OPRO and BO incur ex-
 370 tra cost without meaningfully improv-
 371 ing the solution. Our method does not
 372 require additional ground-truth simu-
 373 lator queries.
 374

375 **Our method delivers substantial reward gains over Direct Query, especially on medium- and**
 376 **easy-difficulty tasks; on harder tasks, it consistently improves success rate.** As shown in Fig-
 377 ure 4, reward improvements are most pronounced in easier scenarios (*Heat 1D*; low-precision *Euler*



378 **Figure 3: Comparison of Single-Turn and Multi-Turn re-
 379 wards for all methods.** Each bar shows the mean reward,
 380 averaged over all precision levels of a task, for methods on
 381 a given base model. As discussed in definition 4.2, OPRO is
 382 only considered in the Multi-Turn scenarios. BO is plotted
 383 alongside LLM methods for clarity of comparison.
 384

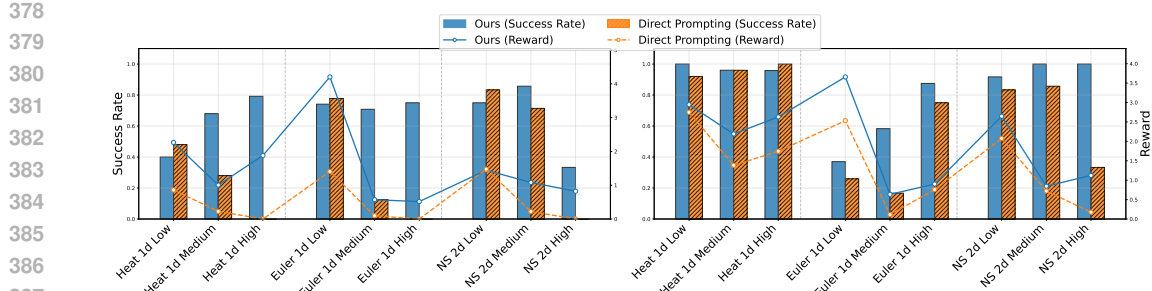


Figure 4: Reward (R^0, R^m) and success rate (P^0, P^m) across all difficulty levels in the Single-Turn setting (left) and the Multi-Turn setting (right). Tasks are ordered by increasing difficulty: *Heat 1d*, *Euler 1d*, *NS Transient 2D*. Our methods improvements in reward are largest on easy-to-medium tasks and remain present on hard tasks.

ID). In harder scenarios (medium- to high-precision *Euler 1D*; *NS Transient 2D*), reward gains are smaller, but success rate improves steadily. This pattern suggests an intrinsic optimization behavior: for unfamiliar questions, *CAED-Agent* first optimizes correctness, and then optimizes efficiency.

4.5 ABLATIONS

We present ablation studies for the two main components of *CAED-Agent*: the surrogate neural network and the LLM agent. All ablation studies are preformed on the same set of problems, *Euler 1D* with medium precision level, with base model OpenAI o4-mini (OpenAI et al., 2024).

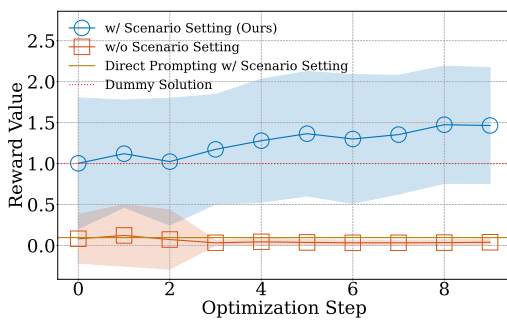


Figure 5: Mean Reward over optimization Steps for *CAED-Agent*, with or without scenario setting description in prompt.

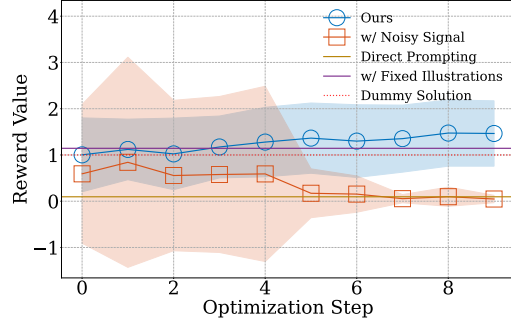


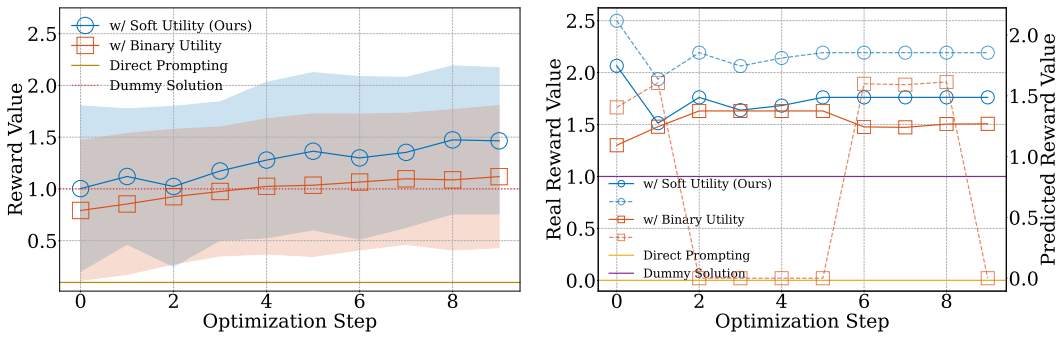
Figure 6: Mean Reward over optimization Steps for *CAED-Agent*, either with surrogate signal, noisy signal or fixed illustrations.

Physics prior knowledge is necessary to achieve in-context optimization in our tasks. Figure 5 presents an ablation study on whether the scenario setting is included in the LLM’s prompt. We argue that the merits of utilizing LLM in our framework lie in both their in-context optimization abilities and their prior domain knowledge. For the alternative setting (orange lines in 5), we only prompt the model to solve the problem as a numerical optimization problem; see the prompts in E. Figure 5 shows that *CAED-Agent* (blue lines), with physics prior knowledge, can consistently improve reward to surpass baselines, whereas the trajectory without scenario description fails to achieve improvements and converges to a low-reward local optimum. This behavior is also visible in a case study illustrated in 11a.

Feedback signals are important for agent optimization in our tasks. We study the effects of our surrogate signal network and present the results in figure 6. We compare *CAED-Agent* with (1) in-context optimization with a fixed set of ground-truth examples for all problems, and (2) our agent equipped with noisy signal from a poorly fitted surrogate model. We experiment on both Single-Turn and Multi-Turn settings in *Euler 1D*’s medium precision level with base model GPT-4o-mini. As shown in Figure 6 and 11b, in both the dataset-level pattern and the case study, our method starts from a worse point than that of fixed illustrations’, but surpasses it in later optimization steps; the noisy signal fails to guide the model’s optimization after the first few steps, highlighting the importance of an effective signal model.

432 **Soft surrogate signals significantly improve optimization performance compared to binary surrogate signals.** We verify the effectiveness of the soft utility (Definition 3.3). Specifically, we compare Single-Turn results of our framework under two variants: (a) integrating surrogates with the original binary utility function, and (b) our approach that uses a soft utility function in the surrogate signals. As shown in Figure 7, the soft-utility variant achieves significantly better performance at the dataset level and exhibits a steadier upward trend in the case study.

433
434
435
436
437
438 We also present a case study in 7b, which plots the predicted reward (**dashed lines**) of the step-wise
439 optimal design for both methods besides the real reward in **solid lines**. As shown by the orange
440 dashed line in 7b, once the model receives a zero-utility signal from the surrogate at step 3, it stops
441 refining and remains at a local optimum. By contrast, the blue line shows that although the model
442 proposes the same point at step 3, the non-zero soft-utility signal it receives enables it to continue
443 refining the solution.



444
445 (a) Mean Reward over Optimization Steps for *CAED-Agent*, using different functions for surrogate signal. (b) Case study. An exemplar optimization trajectory in
446 447 Single-Turn setting. Notations explained in 4.5.
448

449 Figure 7: **Study on soft utility functions vs. binary signals for surrogate signal for o4-mini.**

450 Complete ablation study results are presented in Table 3 of Appendix F. We show that each component
451 of *CAED-Agent*, including the physics prior, the signal NN, and the prompt design all contribute
452 to the final performance. *CAED-Agent* achieves the Pareto optima of success rate and efficiency for
453 all settings, as shown in Figure 1.

454 5 CONCLUSION

455 We presented the Cost-Aware Simulation-Based Experimental Design Agent, a LLM Agent framework
456 for experimental design that focuses on cost-efficiency. Through experiments on three physics
457 simulator environments, each with varying environmental setting and precision requirements, we
458 demonstrated that *CAED-Agent* consistently outperforms both classical Bayesian optimization baselines
459 and state-of-the-art LLM-based optimizers. Our results highlight its ability to achieve high success
460 rates and favorable cost-efficiency trade-offs, even when direct evaluations are prohibitively expensive.
461 Our method introduces the novel contribution of utilizing a low-dimensional cost-efficiency
462 signal neural network, which through our ablation studies we show significantly improves utility of
463 both single-turn and multi-turn experiment design. These findings suggest that *CAED-Agent* provides
464 a practical and scalable path toward deploying agentic frameworks in experiment design in
465 scientific discovery pipelines.

466 Our approach has the following limitations for exploration in future work. The accuracy of *CAED-Agent*
467 depends on the fidelity of the surrogate, which may under-fit in highly complex or noisy experimental
468 landscapes, and requires some degree of human tuning. Moreover, our data sampling strategy
469 does not guarantee the minimization of sampling size while the model converges. Future work
470 can aim to address these limitations by exploring richer surrogate models, adaptive sampling strategies,
471 and tighter coupling between surrogate predictions and target function evaluation to improve
472 the quality of feedback to LLM. Extending *CAED-Agent* to multi-objective, higher-dimensional, or
473 real-world experimental systems will further test its scalability and practical utility, paving the way
474 toward more autonomous and cost-efficient experimental design agents.
475

486 **REPRODUCIBILITY**
 487

488 We evaluate this work on three physics-solver environments that we implemented: *Heat 1D*, *Euler*
 489 *ID*, and *NS Transient 2D* which include solvers, reference solutions, problem sets, and evaluation
 490 pipelines. We plan to extend and organize these into a benchmark to aid the open-source community
 491 in solving **Cost-Aware Simulation-Based Experimental Design (CAED)** better. As the benchmark
 492 is still in progress, our solvers, evaluation pipeline, etc. may not yet be robust enough for convenient
 493 reproduction. Therefore, we consider it appropriate to open-source the code for this work after
 494 acceptance, including not only a (subset) of the aforementioned benchmark but also the neural-
 495 network training, the main framework, and the plotting components.

496
 497 **ETHICS STATEMENT**
 498

499 This work studies cost-aware experimental design agents for physics simulations (e.g., 1D Heat
 500 Conduction and Euler equations) and does not involve human subjects, personal data, or sensitive
 501 attributes. All data are synthetic or standard simulation benchmarks; no personally identifiable
 502 information is used or created. We comply with licenses and usage terms for third-party software
 503 and models; any proprietary APIs were accessed under their respective terms.

504 Potential risks are limited. As our method can improve search efficiency, there is a generic risk
 505 of misuse to optimize unsafe physical systems. To mitigate this, we focus on pedagogical and
 506 widely used benchmark scenarios with explicit constraints and provide documentation intended for
 507 scientific replication rather than domain-specific exploitation.

508 Fairness and demographic bias considerations are not applicable to our setting. The environmental
 509 impact is modest: we train lightweight surrogates on small datasets and use limited inference bud-
 510 gets; we report hardware and runtime details to enable carbon accounting. For reproducibility, we
 511 will release code, configurations, and seeds, and follow standard reporting checklists. We declare no
 512 conflicts of interest and no concurrent submissions related to this work.

513
 514 **THE USE OF LARGE LANGUAGE MODELS**
 515

516 In this work, Large Language Models are primarily used for assisting in polishing the mathematical
 517 formulation in 3.3, explaining the results in 4.5 and generating the plotting code for Figure 1, 3, 4,
 518 5, 6 and 7.

519 They are also used for polishing text in some sections. They were NOT used in research ideation
 520 and/or writing.

522
 523
 524
 525
 526
 527
 528
 529
 530
 531
 532
 533
 534
 535
 536
 537
 538
 539

540 REFERENCES
541

- 542 X. Huan, J. Jagalur, and Y. Marzouk. Optimal experimental design: Formulations and computations.
543 *Acta Numerica*, 33:715840, July 2024. ISSN 1474-0508. doi: 10.1017/s0962492924000023.
544 URL <http://dx.doi.org/10.1017/S0962492924000023>.
- 545 J. D. Anderson, J. Wendt, and . others. *Computational fluid dynamics*, volume 206. Springer, 1995.
- 546 J. Snoek, H. Larochelle, and R. P. Adams. Practical bayesian optimization of machine learning
547 algorithms. *Advances in neural information processing systems*, 25, 2012.
- 548 Y. Yao, F. Liu, J. Cheng, and Q. Zhang. Evolve cost-aware acquisition functions using large language
549 models. In *International Conference on Parallel Problem Solving from Nature*, pages 374–390.
550 Springer, 2024.
- 551 Y. S. Perera, D. Ratnaweera, C. H. Dasanayaka, and C. Abeykoon. The role of artificial intelligence-
552 driven soft sensors in advanced sustainable process industries: A critical review. *Engineering
553 Applications of Artificial Intelligence*, 121:105988, 2023.
- 554 I. Char, Y. Chung, W. Neiswanger, K. Kandasamy, A. O. Nelson, M. Boyer, E. Kolemen, and
555 J. Schneider. Offline contextual bayesian optimization. *Advances in Neural Information Pro-
556 cessing Systems*, 32, 2019.
- 557 B. Trabucco, X. Geng, A. Kumar, and S. Levine. Design-bench: Benchmarks for data-driven of-
558 flne model-based optimization. In *International Conference on Machine Learning*, pages 21658–
559 21676. PMLR, 2022.
- 560 J. C. Fromer and C. W. Coley. An algorithmic framework for synthetic cost-aware decision making
561 in molecular design. *Nature Computational Science*, 4(6):440–450, 2024.
- 562 A. Bharti, D. Huang, S. Kaski, and F. Briol. Cost-aware simulation-based inference. *arXiv preprint
563 arXiv:2410.07930*, 2024.
- 564 . OpenAI, J. Achiam, S. Adler, S. Agarwal, L. Ahmad, I. Akkaya, F. L. Aleman, D. Almeida,
565 J. Altenschmidt, S. Altman, S. Anadkat, R. Avila, I. Babuschkin, S. Balaji, V. Balcom, P. Bal-
566 tescu, H. Bao, M. Bavarian, J. Belgum, I. Bello, J. Berdine, G. Bernadett-Shapiro, C. Berner,
567 L. Bogdonoff, O. Boiko, M. Boyd, A. Brakman, G. Brockman, T. Brooks, M. Brundage, K. But-
568 ton, T. Cai, R. Campbell, A. Cann, B. Carey, C. Carlson, R. Carmichael, B. Chan, C. Chang,
569 F. Chantzis, D. Chen, S. Chen, R. Chen, J. Chen, M. Chen, B. Chess, C. Cho, C. Chu, H. W.
570 Chung, D. Cummings, J. Currier, Y. Dai, C. Decareaux, T. Degry, N. Deutsch, D. Deville, A. Dhar,
571 D. Dohan, S. Dowling, S. Dunning, A. Ecoffet, A. Eleti, T. Eloundou, D. Farhi, L. Fedus, N. Fe-
572 lix, S. P. Fishman, J. Forte, I. Fulford, L. Gao, E. Georges, C. Gibson, V. Goel, T. Gogineni,
573 G. Goh, R. Gontijo-Lopes, J. Gordon, M. Grafstein, S. Gray, R. Greene, J. Gross, S. S. Gu,
574 Y. Guo, C. Hallacy, J. Han, J. Harris, Y. He, M. Heaton, J. Heidecke, C. Hesse, A. Hickey,
575 W. Hickey, P. Hoeschele, B. Houghton, K. Hsu, S. Hu, X. Hu, J. Huizinga, S. Jain, S. Jain,
576 J. Jang, A. Jiang, R. Jiang, H. Jin, D. Jin, S. Jomoto, B. Jonn, H. Jun, T. Kaftan, . Kaiser,
577 A. Kamali, I. Kanitscheider, N. S. Keskar, T. Khan, L. Kilpatrick, J. W. Kim, C. Kim, Y. Kim,
578 J. H. Kirchner, J. Kirov, M. Knight, D. Kokotajlo, . Kondraciuk, A. Kondrich, A. Konstantinidis,
579 K. Kosic, G. Krueger, V. Kuo, M. Lampe, I. Lan, T. Lee, J. Leike, J. Leung, D. Levy, C. M. Li,
580 R. Lim, M. Lin, S. Lin, M. Litwin, T. Lopez, R. Lowe, P. Lue, A. Makanju, K. Malfacini, S. Man-
581 nning, T. Markov, Y. Markovski, B. Martin, K. Mayer, A. Mayne, B. McGrew, S. M. McKinney,
582 C. McLeavey, P. McMillan, J. McNeil, D. Medina, A. Mehta, J. Menick, L. Metz, A. Mishchenko,
583 P. Mishkin, V. Monaco, E. Morikawa, D. Mossing, T. Mu, M. Murati, O. Murk, D. Mély, A. Nair,
584 R. Nakano, R. Nayak, A. Neelakantan, R. Ngo, H. Noh, L. Ouyang, C. O’Keefe, J. Pachocki,
585 A. Paino, J. Palermo, A. Pantuliano, G. Parascandolo, J. Parish, E. Parparita, A. Passos, M. Pavlov,
586 A. Peng, A. Perelman, F. Avila Belbute Peres, M. Petrov, H. P. Oliveira Pinto, . Michael, . Poko-
587 rny, M. Pokrass, V. H. Pong, T. Powell, A. Power, B. Power, E. Proehl, R. Puri, A. Radford,
588 J. Rae, A. Ramesh, C. Raymond, F. Real, K. Rimbach, C. Ross, B. Rotsted, H. Roussez, N. Ryder,
589 M. Saltarelli, T. Sanders, S. Santurkar, G. Sastry, H. Schmidt, D. Schnurr, J. Schulman, D. Sel-
590 sam, K. Sheppard, T. Sherbakov, J. Shieh, S. Shoker, P. Shyam, S. Sidor, E. Sigler, M. Simens,
591 J. Sitkin, K. Slama, I. Sohl, B. Sokolowsky, Y. Song, N. Staudacher, F. P. Such, N. Summers,
592 I. Sutskever, J. Tang, N. Tezak, M. B. Thompson, P. Tillet, A. Tootoonchian, E. Tseng, P. Tuggle,

- 594 N. Turley, J. Tworek, J. F. C. Uribe, A. Vallone, A. Vijayvergiya, C. Voss, C. Wainwright, J. J.
 595 Wang, A. Wang, B. Wang, J. Ward, J. Wei, C. Weinmann, A. Welihinda, P. Welinder, J. Weng,
 596 L. Weng, M. Wiethoff, D. Willner, C. Winter, S. Wolrich, H. Wong, L. Workman, S. Wu, J. Wu,
 597 M. Wu, K. Xiao, T. Xu, S. Yoo, K. Yu, Q. Yuan, W. Zaremba, R. Zellers, C. Zhang, M. Zhang,
 598 S. Zhao, T. Zheng, J. Zhuang, W. Zhuk, and B. Zoph. Gpt-4 technical report, 2024. URL
 599 <https://arxiv.org/abs/2303.08774>.
- 600
- 601 A. Grattafiori, A. Dubey, A. Jauhri, A. Pandey, A. Kadian, A. Al-Dahle, A. Letman, A. Mathur,
 602 A. Schelten, A. Vaughan, A. Yang, A. Fan, A. Goyal, A. Hartshorn, A. Yang, A. Mitra, A. Sravankumar,
 603 A. Korenev, A. Hinsvark, A. Rao, A. Zhang, A. Rodriguez, A. Gregerson, A. Spataru,
 604 B. Roziere, B. Biron, B. Tang, B. Chern, C. Caucheteux, C. Nayak, C. Bi, C. Marra, C. Mc-
 605 Connell, C. Keller, C. Touret, C. Wu, C. Wong, C. C. Ferrer, C. Nikolaidis, D. Allonsius,
 606 D. Song, D. Pintz, D. Livshits, D. Wyatt, D. Esiobu, D. Choudhary, D. Mahajan, D. Garcia-
 607 Olano, D. Perino, D. Hupkes, E. Lakomkin, E. AlBadawy, E. Lobanova, E. Dinan, E. M. Smith,
 608 F. Radenovic, F. Guzmán, F. Zhang, G. Synnaeve, G. Lee, G. L. Anderson, G. Thattai, G. Nail,
 609 G. Mialon, G. Pang, G. Cucurell, H. Nguyen, H. Korevaar, H. Xu, H. Touvron, I. Zarov, I. A.
 610 Ibarra, I. Kloumann, I. Misra, I. Evtimov, J. Zhang, J. Copet, J. Lee, J. Geffert, J. Vranes, J. Park,
 611 J. Mahadeokar, J. Shah, J. Linde, J. Billock, J. Hong, J. Lee, J. Fu, J. Chi, J. Huang, J. Liu,
 612 J. Wang, J. Yu, J. Bitton, J. Spisak, J. Park, J. Rocca, J. Johnstun, J. Saxe, J. Jia, K. V. Alwala,
 613 K. Prasad, K. Upasani, K. Plawiak, K. Li, K. Heafield, K. Stone, K. El-Arini, K. Iyer, K. Ma-
 614 lik, K. Chiu, K. Bhalla, K. Lakhotia, L. Rantala-Yeary, L. Maaten, L. Chen, L. Tan, L. Jenkins,
 615 L. Martin, L. Madaan, L. Malo, L. Blecher, L. Landzaat, L. Oliveira, M. Muzzi, M. Pasupuleti,
 616 M. Singh, M. Paluri, M. Kardas, M. Tsimpoukelli, M. Oldham, M. Rita, M. Pavlova, M. Kam-
 617 badur, M. Lewis, M. Si, M. K. Singh, M. Hassan, N. Goyal, N. Torabi, N. Bashlykov, N. Bo-
 618 goychev, N. Chatterji, N. Zhang, O. Duchenne, O. Celebi, P. Alrassy, P. Zhang, P. Li, P. Vasic,
 619 P. Weng, P. Bhargava, P. Dubal, P. Krishnan, P. S. Koura, P. Xu, Q. He, Q. Dong, R. Srinivasan,
 620 R. Ganapathy, R. Calderer, R. S. Cabral, R. Stojnic, R. Raileanu, R. Maheswari, R. Girdhar,
 621 R. Patel, R. Sauvestre, R. Polidoro, R. Sumbaly, R. Taylor, R. Silva, R. Hou, R. Wang, S. Hos-
 622 seini, S. Chennabasappa, S. Singh, S. Bell, S. S. Kim, S. Edunov, S. Nie, S. Narang, S. Raparthy,
 623 S. Shen, S. Wan, S. Bhosale, S. Zhang, S. Vandenhende, S. Batra, S. Whitman, S. Sootla, S. Col-
 624 lot, S. Gururangan, S. Borodinsky, T. Herman, T. Fowler, T. Sheasha, T. Georgiou, T. Scialom,
 625 T. Speckbacher, T. Mihaylov, T. Xiao, U. Karn, V. Goswami, V. Gupta, V. Ramanathan, V. Kerkez,
 626 V. Gonguet, V. Do, V. Vogeti, V. Albiero, V. Petrovic, W. Chu, W. Xiong, W. Fu, W. Meers, X. Mar-
 627 tinet, X. Wang, X. Wang, X. E. Tan, X. Xia, X. Xie, X. Jia, X. Wang, Y. Goldschlag, Y. Gaur,
 628 Y. Babaei, Y. Wen, Y. Song, Y. Zhang, Y. Li, Y. Mao, Z. D. Coudert, Z. Yan, Z. Chen, Z. Papakipos,
 629 A. Singh, A. Srivastava, A. Jain, A. Kelsey, A. Shajnfeld, A. Gangidi, A. Victoria, A. Goldstand,
 630 A. Menon, A. Sharma, A. Boesenberg, A. Baevski, A. Feinstein, A. Kallet, A. Sangani, A. Teo,
 631 A. Yunus, A. Lupu, A. Alvarado, A. Caples, A. Gu, A. Ho, A. Poulton, A. Ryan, A. Ramchandani,
 632 A. Dong, A. Franco, A. Goyal, A. Saraf, A. Chowdhury, A. Gabriel, A. Bharambe, A. Eisenman,
 633 A. Yazdan, B. James, B. Maurer, B. Leonhardi, B. Huang, B. Loyd, B. D. Paola, B. Paranjape,
 634 B. Liu, B. Wu, B. Ni, B. Hancock, B. Wasti, B. Spence, B. Stojkovic, B. Gamido, B. Montalvo,
 635 C. Parker, C. Burton, C. Mejia, C. Liu, C. Wang, C. Kim, C. Zhou, C. Hu, C. Chu, C. Cai, C. Tin-
 636 dal, C. Feichtenhofer, C. Gao, D. Civin, D. Beaty, D. Kreymer, D. Li, D. Adkins, D. Xu, D. Tes-
 637 tuggine, D. David, D. Parikh, D. Liskovich, D. Foss, D. Wang, D. Le, D. Holland, E. Dowling,
 638 E. Jamil, E. Montgomery, E. Presani, E. Hahn, E. Wood, E. Le, E. Brinkman, E. Arcaute, E. Dun-
 639 bar, E. Smothers, F. Sun, F. Kreuk, F. Tian, F. Kokkinos, F. Ozgenel, F. Caggioni, F. Kanayet,
 640 F. Seide, G. M. Florez, G. Schwarz, G. Badeer, G. Swee, G. Halpern, G. Herman, G. Sizov,
 641 . Guanyi, . Zhang, G. Lakshminarayanan, H. Inan, H. Shojanazeri, H. Zou, H. Wang, H. Zha,
 642 H. Habeeb, H. Rudolph, H. Suk, H. Asperegren, H. Goldman, H. Zhan, I. Damlaj, I. Molybog,
 643 I. Tufanov, I. Leontiadis, I. Veliche, I. Gat, J. Weissman, J. Geboski, J. Kohli, J. Lam, J. Asher,
 644 J. Gaya, J. Marcus, J. Tang, J. Chan, J. Zhen, J. Reizenstein, J. Teboul, J. Zhong, J. Jin, J. Yang,
 645 J. Cummings, J. Carvill, J. Shepard, J. McPhie, J. Torres, J. Ginsburg, J. Wang, K. Wu, K. H. U,
 646 K. Saxena, K. Khandelwal, K. Zand, K. Matosich, K. Veeraraghavan, K. Michelena, K. Li, K. Ja-
 647 gadeesh, K. Huang, K. Chawla, K. Huang, L. Chen, L. Garg, L. A. L. Silva, L. Bell, L. Zhang,
 648 L. Guo, L. Yu, L. Moshkovich, L. Wehrstedt, M. Khabsa, M. Avalani, M. Bhatt, M. Mankus,
 649 M. Hasson, M. Lennie, M. Reso, M. Groshev, M. Naumov, M. Lathi, M. Keneally, M. Liu, M. L.
 650 Seltzer, M. Valko, M. Restrepo, M. Patel, M. Vyatskov, M. Samvelyan, M. Clark, M. Macey,
 651 M. Wang, M. J. Hermoso, M. Metanat, M. Rastegari, M. Bansal, N. Santhanam, N. Parks,
 652 N. White, N. Bawa, N. Singhal, N. Usunier, N. Mehta, N. P. Laptev, N. Dong, N. Cheng,

- 648 O. Chernoguz, O. Hart, O. Salpekar, O. Kalinli, P. Kent, P. Parekh, P. Saab, P. Balaji, P. Rittner,
 649 P. Bontrager, P. Roux, P. Dollar, P. Zvyagina, P. Ratanchandani, P. Yuvraj, Q. Liang, R. Alao,
 650 R. Rodriguez, R. Ayub, R. Murthy, R. Nayani, R. Mitra, R. Parthasarathy, R. Li, R. Hogan, R. Bat-
 651 ttey, R. Wang, R. Howes, R. Rinott, S. Mehta, S. Siby, S. J. Bondu, S. Datta, S. Chugh, S. Hunt,
 652 S. Dhillon, S. Sidorov, S. Pan, S. Mahajan, S. Verma, S. Yamamoto, S. Ramaswamy, S. Lindsay,
 653 S. Lindsay, S. Feng, S. Lin, S. C. Zha, S. Patil, S. Shankar, S. Zhang, S. Zhang, S. Wang, S. Agar-
 654 wal, S. Sajuyigbe, S. Chintala, S. Max, S. Chen, S. Kehoe, S. Satterfield, S. Govindaprasad,
 655 S. Gupta, S. Deng, S. Cho, S. Virk, S. Subramanian, S. Choudhury, S. Goldman, T. Remez,
 656 T. Glaser, T. Best, T. Koehler, T. Robinson, T. Li, T. Zhang, T. Matthews, T. Chou, T. Shaked,
 657 V. Vontimitta, V. Ajayi, V. Montanez, V. Mohan, V. S. Kumar, V. Mangla, V. Ionescu, V. Poe-
 658 naru, V. T. Mihailescu, V. Ivanov, W. Li, W. Wang, W. Jiang, W. Bouaziz, W. Constable, X. Tang,
 659 X. Wu, X. Wang, X. Wu, X. Gao, Y. Kleinman, Y. Chen, Y. Hu, Y. Jia, Y. Qi, Y. Li, Y. Zhang,
 660 Y. Zhang, Y. Adi, Y. Nam, . Yu, . Wang, Y. Zhao, Y. Hao, Y. Qian, Y. Li, Y. He, Z. Rait, Z. DeVito,
 661 Z. Rosnbrick, Z. Wen, Z. Yang, Z. Zhao, and Z. Ma. The llama 3 herd of models, 2024. URL
<https://arxiv.org/abs/2407.21783>.
- 662 . DeepSeek-AI, A. Liu, B. Feng, B. Xue, B. Wang, B. Wu, C. Lu, C. Zhao, C. Deng, C. Zhang,
 663 C. Ruan, D. Dai, D. Guo, D. Yang, D. Chen, D. Ji, E. Li, F. Lin, F. Dai, F. Luo, G. Hao, G. Chen,
 664 G. Li, H. Zhang, H. Bao, H. Xu, H. Wang, H. Zhang, H. Ding, H. Xin, H. Gao, H. Li, H. Qu, J. L.
 665 Cai, J. Liang, J. Guo, J. Ni, J. Li, J. Wang, J. Chen, J. Chen, J. Yuan, J. Qiu, J. Li, J. Song, K. Dong,
 666 K. Hu, K. Gao, K. Guan, K. Huang, K. Yu, L. Wang, L. Zhang, L. Xu, L. Xia, L. Zhao, L. Wang,
 667 L. Zhang, M. Li, M. Wang, M. Zhang, M. Zhang, M. Tang, M. Li, N. Tian, P. Huang, P. Wang,
 668 P. Zhang, Q. Wang, Q. Zhu, Q. Chen, Q. Du, R. J. Chen, R. L. Jin, R. Ge, R. Zhang, R. Pan,
 669 R. Wang, R. Xu, R. Zhang, R. Chen, S. S. Li, S. Lu, S. Zhou, S. Chen, S. Wu, S. Ye, S. Ye, S. Ma,
 670 S. Wang, S. Zhou, S. Yu, S. Zhou, S. Pan, T. Wang, T. Yun, T. Pei, T. Sun, W. L. Xiao, W. Zeng,
 671 W. Zhao, W. An, W. Liu, W. Liang, W. Gao, W. Yu, W. Zhang, X. Q. Li, X. Jin, X. Wang, X. Bi,
 672 X. Liu, X. Wang, X. Shen, X. Chen, X. Zhang, X. Chen, X. Nie, X. Sun, X. Wang, X. Cheng,
 673 X. Liu, X. Xie, X. Liu, X. Yu, X. Song, X. Shan, X. Zhou, X. Yang, X. Li, X. Su, X. Lin, Y. K. Li,
 674 Y. Q. Wang, Y. X. Wei, Y. X. Zhu, Y. Zhang, Y. Xu, Y. Xu, Y. Huang, Y. Li, Y. Zhao, Y. Sun, Y. Li,
 675 Y. Wang, Y. Yu, Y. Zheng, Y. Zhang, Y. Shi, Y. Xiong, Y. He, Y. Tang, Y. Piao, Y. Wang, Y. Tan,
 676 Y. Ma, Y. Liu, Y. Guo, Y. Wu, Y. Ou, Y. Zhu, Y. Wang, Y. Gong, Y. Zou, Y. He, Y. Zha, Y. Xiong,
 677 Y. Ma, Y. Yan, Y. Luo, Y. You, Y. Liu, Y. Zhou, Z. F. Wu, Z. Z. Ren, Z. Ren, Z. Sha, Z. Fu, Z. Xu,
 678 Z. Huang, Z. Zhang, Z. Xie, Z. Zhang, Z. Hao, Z. Gou, Z. Ma, Z. Yan, Z. Shao, Z. Xu, Z. Wu,
 679 Z. Zhang, Z. Li, Z. Gu, Z. Zhu, Z. Liu, Z. Li, Z. Xie, Z. Song, Z. Gao, and Z. Pan. Deepseek-v3
 680 technical report, 2025. URL <https://arxiv.org/abs/2412.19437>.
- 681 S. Ren, P. Jian, Z. Ren, C. Leng, C. Xie, and J. Zhang. Towards scientific intelligence: A survey of
 682 llm-based scientific agents, 2025. URL <https://arxiv.org/abs/2503.24047>.
- 683 M. Zhong, C. An, W. Chen, J. Han, and P. He. Seeking neural nuggets: Knowledge transfer in large
 684 language models from a parametric perspective, 2024. URL <https://arxiv.org/abs/2310.11451>.
- 685 Q. Lv, T. Liu, and H. Wang. Exploiting edited large language models as general scientific optimizers.
 686 *arXiv preprint arXiv:2503.09620*, 2025.
- 687 Y. Roohani, A. Lee, Q. Huang, J. Vora, Z. Steinhart, K. Huang, A. Marson, P. Liang, and J. Leskovec.
 688 Biodiscoveryagent: An ai agent for designing genetic perturbation experiments, 2025. URL
 689 <https://arxiv.org/abs/2405.17631>.
- 690 T. Liu, N. Astorga, N. Seedat, and M. Schaar. Large language models to enhance bayesian optimiza-
 691 tion, 2024. URL <https://arxiv.org/abs/2402.03921>.
- 692 Y. Chen, X. Song, C. Lee, Z. Wang, R. Zhang, D. Dohan, K. Kawakami, G. Kochanski, A. Doucet,
 693 M. Ranzato, and . others. Towards learning universal hyperparameter optimizers with transform-
 694 ers. *Advances in Neural Information Processing Systems*, 35:32053–32068, 2022.
- 695 X. Song, O. Li, C. Lee, B. Yang, D. Peng, S. Perel, and Y. Chen. Omnipred: Language models as
 696 universal regressors. *arXiv preprint arXiv:2402.14547*, 2024.
- 697 E. Tang, B. Yang, and X. Song. Understanding llm embeddings for regression, 2025. URL
 698 <https://arxiv.org/abs/2411.14708>.

- 702 D. Wu, J. Wang, Y. Meng, Y. Zhang, L. Sun, and Z. Wang. Catp-llm: Empowering large language
 703 models for cost-aware tool planning. *arXiv preprint arXiv:2411.16313*, 2024.
- 704
- 705 B. Lyu, Y. Cao, D. Watson-Parris, L. Bergen, T. Berg-Kirkpatrick, and R. Yu. Adapting while
 706 learning: Grounding llms for scientific problems with intelligent tool usage adaptation. *arXiv
 707 preprint arXiv:2411.00412*, 2024.
- 708
- 709 C. Yang, X. Wang, Y. Lu, H. Liu, Q. V. Le, D. Zhou, and X. Chen. Large language models as
 710 optimizers. In *The Twelfth International Conference on Learning Representations*, 2023.
- 711
- 712 F. Nogueira. Bayesian optimization: Open source constrained global optimization tool for python.
 https://github.com/bayesian-optimization/BayesianOptimization,
 713 2014. Accessed: 2025-08-25.
- 714
- 715 B. Smucker, M. Krzywinski, and N. Altman. Optimal experimental design. *Nat. Methods*, 15(8):
 559–560, 2018.
- 716
- 717 M. D. Knudsen, L. Georges, K. S. Skeie, and S. Petersen. Experimental test of a black-box economic
 718 model predictive control for residential space heating. *Applied energy*, 298:117227, 2021.
- 719
- 720 P. Pandita. *Bayesian Optimal Design of Experiments for Expensive Black-Box Functions Under
 Uncertainty*. PhD thesis, Purdue University, 2019.
- 721
- 722 G. Daras, H. Chung, C. Lai, Y. Mitsufuji, J. C. Ye, P. Milanfar, A. G. Dimakis, and M. Delbracio. A
 723 survey on diffusion models for inverse problems. *arXiv preprint arXiv:2410.00083*, 2024.
- 724
- 725 H. Zheng, W. Chu, B. Zhang, Z. Wu, A. Wang, B. T. Feng, C. Zou, Y. Sun, N. Kovachki, Z. E. Ross,
 726 and . others. Inversebench: Benchmarking plug-and-play diffusion priors for inverse problems in
 727 physical sciences. *arXiv preprint arXiv:2503.11043*, 2025a.
- 728
- 729 B. Wang, G. Duan, W. Lv, Y. Tao, H. Xiong, D. Zhang, G. Yang, and F. Shu. Design and exper-
 730 imental realization of triple-band electromagnetically induced transparency terahertz metamateri-
 731 als employing two big-bright modes for sensing applications. *Nanoscale*, 15(45):18435–18446,
 2023.
- 732
- 733 C. Lu, C. Lu, R. T. Lange, J. Foerster, J. Clune, and D. Ha. The ai scientist: Towards fully automated
 open-ended scientific discovery. *arXiv preprint arXiv:2408.06292*, 2024.
- 734
- 735 D. A. Boiko, R. MacKnight, B. Kline, and G. Gomes. Autonomous chemical research with large
 736 language models. *Nature*, 624(7992):570–578, 2023.
- 737
- 738 T. Zheng, Z. Deng, H. T. Tsang, W. Wang, J. Bai, Z. Wang, and Y. Song. From automation to auton-
 739 omy: A survey on large language models in scientific discovery. *arXiv preprint arXiv:2505.13259*,
 2025b.
- 740
- 741 D. Wang, Y. Wang, X. Jiang, Y. Zhang, Y. Pang, and M. Zhang. When large language models meet
 742 optical networks: paving the way for automation. *Electronics*, 13(13):2529, 2024.
- 743
- 744 A. M. Bran, S. Cox, O. Schilter, C. Baldassari, A. D. White, and P. Schwaller. Chemcrow: Aug-
 745 menting large-language models with chemistry tools. *arXiv preprint arXiv:2304.05376*, 2023.
- 746
- 747 K. M. Jablonka, P. Schwaller, A. Ortega-Guerrero, and B. Smit. Leveraging large language models
 748 for predictive chemistry. *Nature Machine Intelligence*, 6(2):161–169, 2024.
- 749
- 750 J. S. Chan, N. Chowdhury, O. Jaffe, J. Aung, D. Sherburn, E. Mays, G. Starace, K. Liu, L. Maksin,
 751 T. Patwardhan, L. Weng, and A. Mdry. Mle-bench: Evaluating machine learning agents on ma-
 752 chine learning engineering, 2025. URL <https://arxiv.org/abs/2410.07095>.
- 753
- 754 H. Hao, X. Zhang, and A. Zhou. Large language models as surrogate models in evolutionary algo-
 755 rithms: A preliminary study. *Swarm and Evolutionary Computation*, 91:101741, 2024.
- 756
- P. Ghafariasl, A. Mahmoudan, M. Mohammadi, A. Nazarpourvar, S. Hoseinzadeh, M. Fathali,
 757 S. Chang, M. Zeinalnezhad, and D. A. Garcia. Neural network-based surrogate modeling and
 758 optimization of a multigeneration system. *Applied Energy*, 364:123130, 2024.

- 756 D. Hou and R. Evins. A protocol for developing and evaluating neural network-based surrogate
757 models and its application to building energy prediction. *Renewable and Sustainable Energy*
758 *Reviews*, 193:114283, 2024.
- 759 C. E. Rasmussen. *Gaussian Processes in Machine Learning*, pages 63–71. Springer Berlin Heidel-
760 berg, Berlin, Heidelberg, 2004. ISBN 978-3-540-28650-9. doi: 10.1007/978-3-540-28650-9_4.
761 URL https://doi.org/10.1007/978-3-540-28650-9_4.
- 762 J. Berk, S. Gupta, S. Rana, and S. Venkatesh. Randomised gaussian process upper confidence bound
763 for bayesian optimisation, 2020. URL <https://arxiv.org/abs/2006.04296>.

765
766
767
768
769
770
771
772
773
774
775
776
777
778
779
780
781
782
783
784
785
786
787
788
789
790
791
792
793
794
795
796
797
798
799
800
801
802
803
804
805
806
807
808
809

810 A EXPERIMENTAL ENVIRONMENT 811

812 **Heat Transfer 1D. (*Heat ID*)** This solver addresses the 1D heat conduction equation:

$$813 \quad 814 \quad \frac{\partial T}{\partial t} = \alpha \frac{\partial^2 T}{\partial x^2}$$

816 using explicit finite difference methods with natural convection boundary conditions at $x = 0$ and
817 adiabatic conditions at $x = L$. The tunable parameters include the spatial resolution (`n_space`)
818 and the CFL number (`cfl`) that determines the simulation time step by:

$$819 \quad 820 \quad \Delta t = cfl \times \frac{(\Delta x)^2}{2\alpha},$$

821 where α is the thermal diffusivity. The computational cost follows the relationship $C = n_space \times$
822 n_t , where n_t is the number of time steps accumulated in the solver. The metric for convergence
823 is the RMSE of the heat flux at the convection boundary at the final time step. This simulation has
824 25 different profiles with varying initial uniform temperatures and physical properties, generating
825 148 tasks in total, counting both Single-Turn and Multi-Turn settings.

826 **Euler 1D. (*Euler ID*)** This solver implements the 1D Euler equations for compressible flow:

$$827 \quad 828 \quad \frac{\partial \mathbf{U}}{\partial t} + \frac{\partial \mathbf{F}(\mathbf{U})}{\partial x} = 0$$

831 using the MUSCL-Roe method with superbee limiter for high-resolution shock capturing. The tun-
832 able parameters include the CFL number (`cfl`) that determines the simulation time step by:

$$833 \quad 834 \quad \Delta t = cfl \times \frac{\Delta x}{|\lambda|_{\max}},$$

835 where $|\lambda|_{\max}$ is the maximum eigenvalue of the flux Jacobian, the spatial resolution (`n_space`), the
836 limiter parameter `beta` for generalized minmod flux limiter, and the blending parameter `k` between
837 0-th and 1-st order interpolation scheme. The computational cost follows the relationship $C =$
838 $n_space \times n_t$, where n_t is the number of time steps accumulated in the solver. Convergence
839 is evaluated through multiple criteria: RMSE of the solution fields, positivity preservation of density
840 and pressure, and shock consistency validation. The dataset encompasses 3 classical benchmark
841 profiles (Sod shock tube, Lax problem, and Mach 3), generating a total of 134 tasks, counting both
842 Single-Turn and Multi-Turn settings.

843 **Transient Navier-Stokes 2D. (*NS Transient 2D*)** This solver implements the 2D transient incom-
844 pressible Navier-Stokes equations:

$$845 \quad \frac{\partial u}{\partial x} + \frac{\partial v}{\partial y} = 0$$

$$846 \quad \frac{\partial u}{\partial t} + u \frac{\partial u}{\partial x} + v \frac{\partial u}{\partial y} = -\frac{\partial p}{\partial x} + \frac{1}{Re} \left(\frac{\partial^2 u}{\partial x^2} + \frac{\partial^2 u}{\partial y^2} \right)$$

$$847 \quad \frac{\partial v}{\partial t} + u \frac{\partial v}{\partial x} + v \frac{\partial v}{\partial y} = -\frac{\partial p}{\partial y} + \frac{1}{Re} \left(\frac{\partial^2 v}{\partial x^2} + \frac{\partial^2 v}{\partial y^2} \right)$$

848 where u, v are velocity components, p is pressure, and Re is the Reynolds number. The tunable
849 parameters include the spatial resolution (`resolution`) that determines the computational grid
850 size, the CFL number (`cfl`) controlling time step stability through $\Delta t = cfl \times \Delta x$, the relaxation
851 factor (`relaxation_factor`) for pressure correction convergence, and the residual threshold
852 (`residual_threshold`) for pressure solver convergence. The computational cost follows the
853 relationship $C = 2 \times \text{resolution}^2 \times (\text{num_steps} + \text{total_pressure_iterations})$,
854 where the factor of 2 accounts for the fixed aspect ratio domain configuration with `x_resolution` =
855 $2 \times \text{resolution}$. Convergence is evaluated through normalized velocity RMSE criteria, with
856 temporal evolution tracked throughout the simulation. The dataset encompasses 18 benchmark
857 profiles across 6 different boundary conditions (simple circular obstacles, complex geometries, random
858 obstacle fields, dual inlet/outlet configurations, dense obstacle arrays, and dragon-shaped obstacles)
859 tested at three Reynolds numbers ($Re=1000, 3000, 6000$), generating a total of 44 tasks across dif-
860 ferent precision levels and geometric complexities.

864 **Dummy Solution Search.** For each task, we find optimal solutions that meet both accuracy requirements and have the lowest cost using brute-force search. Given our parameters have a monotonic relationship between cost and accuracy (i.e., they are spatial resolution), we start with a coarse value and Multi-Turnly refine it with fixed ratios (e.g., halve the time step size, double the spatial resolution) until the distance between adjacent runs is within the accuracy threshold. For single-turn tasks, we set the reference cost to the optimal cost found by brute-force search. For multi-turn tasks, we set the reference cost to the accumulated cost incurred during the brute-force search.
 865
 866
 867
 868
 869
 870

872 B ALGORITHMIC DIAGRAM 873

874 **Algorithm 1** *Solve*, Single-Turn CAED-Agent Framework

875 1: **Input:** Forward experimental process \mathcal{F} , design space \mathcal{X} , environment parameters θ , neural
 876 surrogate \mathcal{S} , number of iteration N , history context length K , initial sample size m .
 877 2: Initialize LLM design-value history as a priority queue \mathcal{M}
 878 3: Push to \mathcal{M} uniformly sampled initial design-value pairs $\{(x_j, \Phi_j^{pred}, \hat{\mathbf{C}}_j^{pred})\}_{j=1}^m$, evaluated by
 879 \mathcal{S}
 880 4: **repeat**
 881 5: LLM proposes candidate designs $\{x_i\}_{i=1}^k$
 882 6: Evaluate candidates with neural surrogate: $(\Phi_i^{pred}, \hat{\mathbf{C}}_i^{pred}) \leftarrow \mathcal{S}(x_i, \theta)$ for $i = 1, \dots, k$
 883 7: Push $\{(x_i, \Phi_i^{pred}, \hat{\mathbf{C}}_i^{pred})\}$ to \mathcal{M} , keeping only top- K samples.
 884 8: **until** Number of iterations N reached
 885 9: **Output:** $x^* = \arg \max_{x_i} \frac{\Phi(\mathcal{S}(x_i, \theta), \theta)}{\mathbf{C}'(x_i, \theta)}$ from design-value history.
 886

887 888 **Algorithm 2** Multi-Turn CAED-Agent Framework

889 1: **Input:** Forward experimental process \mathcal{F} , design space \mathcal{X} , environment parameters θ , neural
 890 surrogate \mathcal{S} , number of iteration for Single-Turn solution N , history context length K , initial
 891 sample size m , maximum allowed number of ground-truth evaluation T .
 892 2: Obtain Single-Turn solution $x = \text{Solve}(\mathcal{F}, \mathcal{X}, \theta, \mathcal{S}, N, K, m)$
 893 3: Initialize solution sequence as a queue $\mathcal{A} = \{x_0\}$
 894 4: Initialize LLM ground-truth design-value history as a priority queue \mathcal{M}
 895 5: Evaluate with ground-truth simulator $(\Phi_0^{gt}, \hat{\mathbf{C}}_0^{gt}) \leftarrow \mathcal{F}(\emptyset, \theta)$
 896 6: Push $(x_0, \Phi_0^{gt}, \hat{\mathbf{C}}_0^{gt})$ to \mathcal{M}
 897 7: **repeat**
 898 8: LLM agent proposes candidate designs $\{x_i\}_{i=1}^k$
 899 9: Evaluate candidates with neural surrogate: $(\Phi_i^{pred}, \hat{\mathbf{C}}_i^{pred}) \leftarrow \mathcal{S}(x_i, \theta)$ for $i = 1, \dots, k$
 900 10: Add top surrogate-evaluated pair $(x_i, \Phi_i^{pred}, \hat{\mathbf{C}}_i^{pred})$ to solution sequence \mathcal{A}
 901 11: Evaluate with ground-truth simulator $(\Phi_i^{gt}, \hat{\mathbf{C}}_i^{gt}) \leftarrow \mathcal{F}(x_i, \theta)$
 902 12: Push $\{(x_i, \Phi_i^{gt}, \hat{\mathbf{C}}_i^{gt})\}$ to \mathcal{M} , keeping only top-K samples
 903 13: **until** LLM outputs *should_stop* = *True* or number of iterations reaches T
 904 14: Outputs \mathcal{A}

905 906 C NEURAL NETWORK TRAINING

909 We train one neural-network for each problem (*Heat 1D*, *Euler 1D*, *NS Transient 2D*)’s all precision
 910 levels; each network’s input and output dimension are as described in 3.2.

911 We uniformly sample design and environmental parameters on coarse grids. We specifically in-
 912 clude environmental parameters to enable interpolation across conditions while avoiding training
 913 and tracking multiple network instances for different environment combinations. We provide the
 914 range of inputs (environmental parameters and tunable parameters) as follows, from which we per-
 915 formed uniform sampling, and statistics of sampled targets in Table 1. We stress that while our
 916 target dimensions have drastically different ranges and high variance, we perform in-dimension nor-
 917 malization as shown in Figure 9, therefore achieving satisfactory training results shown in Figure
 918 8.

```

918
919
Heat 1D:
920  Environmental Parameters:
921    L: [0.1, 0.3] # Wall thickness [m] - uniform random in range
922    k: [0.5, 1.0] # Thermal conductivity [W/m-K] - uniform random in
923    # range
924    h: [0.1, 10000] # Convection coefficient [W/mš-K] - log-uniform
925    # random in range
926    rho: [1000, 2000] # Density [kg/mš] - uniform random in range
927    cp: [800, 1000] # Specific heat [J/kg-K] - uniform random in range
928    T_inf: [-40, 40] # Ambient temperature [řC] - uniform random in
929    # range
930    T_init: [0, 30] # Initial temperature [řC] - uniform random in
931    # range
932    record_dt: 10.0 # Time interval between recordings [s] - fixed
933    end_frame: 24 # Simulation end frames - fixed
934
935
936  Euler 1D:
937  Environmental Parameters:
938    L: 1.0 # Domain length - fixed
939    gamma: 1.4 # Ratio of specific heats - fixed
940    case: {"sod", "lax", "mach_3"} # Initial condition name - 3
941    # discrete values across profiles
942    record_dt: {0.02, 0.012, 0.009} # Time interval between recordings
943    # - specific values per case
944    end_frame: 10 # Simulation end frames - fixed
945
946  Tunable Parameters:
947    n_space: [256, 4096] # Number of grid cells (iterative search:
948    # initial=256, factor=2, max_iter=7)
949
950  NS Transient 2D:
951  Environmental Parameters:
952    boundary_condition: {1, 2, 3, 4, 5, 6} # 6 boundary condition types
953    # across 18 profiles
954    reynolds_num: {1000, 3000, 6000} # Reynolds number - 3 discrete
955    # values
956    vorticity_confinement: 0.0 # Fixed across profiles
957    total_runtime: 1.0 # Fixed across profiles - fixed
958    no_dye: False # Fixed across profiles
959    cpu: False # Fixed across profiles
960    visualization: 0 # Fixed across profiles
961    advection_scheme: "cip" # Fixed across profiles
962
963  Tunable Parameters:
964    resolution: [50, 400] # Grid resolution (iterative search:
965    # initial=50, factor=2, max_iter=4)

```

Table 1: Dataset Statistics.

	<i>RMSE Loss</i>	<i>Cost</i>	<i>N. samples</i>
<i>Heat ID</i>	$4.47e^{-4} \pm 9.50e^{-4}$	$8.33e^7 \pm 1.27e^8$	4440
<i>Euler 1D</i>	$3.48e^{-2} \pm 3.60e^{-2}$	$2.76e^6 \pm 2.42e^6$	4020
<i>NS Transient 2D</i>	$2.55e^{-1} \pm 1.90e^{-1}$	$2.11e^8 \pm 1.94e^8$	1320

For all problems, we train neural-network with the same structure as shown in 9; to achieve optimal results for individual problems, we compare the training results with three sets of structures for

972 each problem and choose the one with the best test loss. Specifically, we experiment with the
 973 combinations of :

```
975
976   h: {2, 3, 4, 6}
977   d: {64, 128, 256}
```

979 Where h, d follow the notation in 9, and the hyper-parameters we used are shown as follows:
 980

```
981
982   activation_mod: ReLU
983   layer_norm: False
984   res_connection: False
985
986   batch: 16
987   epochs: 40
988   steps_per_epoch: 200
989
990   peak_lr: 1e-3
991   weight_decay: 1e-4
992   warmup_steps: 100
993   decay_steps: 1000
994   gnorm_clip: 1.0
995   accumulation_steps: 100
```

996 We show the results of our best checkpoints for the three problems in 8.
 997

D SOFT UTILITY FUNCTION

1000 *Proof of Proposition 3.5.* Let $b(y, \theta) := \mathbf{1}\{\Phi(y, \theta) = 1\}$ be the binary utility and let $s_f(y, \theta) :=$
 1001 $f(y, \theta)$ be any soft utility satisfying Definition 3.3. By *normalization* (Def. 3.3(ii)), $f(y, \theta) \in [0, 1]$,
 1002 and by *feasibility calibration* (Def. 3.3(i)), $f(y, \theta) = 1$ iff $y \in \mathcal{G}_\theta = \{y : \Phi(y, \theta) = 1\}$ and
 1003 $\sup_{y \notin \mathcal{G}_\theta} f(y, \theta) < 1$. Hence the postprocessing map

$$1004 \quad \tau : [0, 1] \rightarrow \{0, 1\}, \quad \tau(u) := \mathbf{1}\{u = 1\}$$

1005 is well-defined (by normalization) and satisfies $b(y, \theta) = \tau(f(y, \theta))$ for all (y, θ) (by feasibility
 1006 calibration). Thus the binary signal is a deterministic garbling of the soft signal.
 1007

1008 Fix a base model and budget $T \geq 1$, and write the histories $h_{t-1}^{\text{bin}} = \{(x_s, y_s, b(y_s, \theta))\}_{s=1}^{t-1}$ and
 1009 $h_{t-1}^f = \{(x_s, y_s, f(y_s, \theta))\}_{s=1}^{t-1}$; then $h_{t-1}^{\text{bin}} = \tau(h_{t-1}^f)$ coordinate-wise. Given any binary-utility
 1010 policy π_{bin} , define a soft-signal policy $\tilde{\pi}_f$ that *simulates* it via

$$1011 \quad \tilde{\pi}_f(\cdot | \theta, h_{t-1}^f) := \pi_{\text{bin}}(\cdot | \theta, \tau(h_{t-1}^f)).$$

1012 Under identical environment randomness, $\tilde{\pi}_f$ induces the same trajectory distribution as π_{bin} , hence

$$1013 \quad \mathbb{E}_{x_T \sim \tilde{\pi}_f(\cdot | \theta)}[R^0(x_T, \theta)] = \mathbb{E}_{x_T \sim \pi_{\text{bin}}(\cdot | \theta)}[R^0(x_T, \theta)] \quad \text{for all } \theta.$$

1014 Taking expectation over the task distribution yields equality in expectation.

1015 By *monotone alignment* (Def. 3.3(iii)), if $\Phi(y_1, \theta) \preceq \Phi(y_2, \theta)$ then $f(y_1, \theta) \leq f(y_2, \theta)$; hence
 1016 ranking by f is orderpreserving with respect to Φ . Since $R^0(x, \theta)$ (Eq. (4)) is nondecreasing in Φ
 1017 (its numerator) and $f = 1$ iff $\Phi = 1$ (by feasibility calibration), using f to refine decisions cannot
 1018 decrease the expected reward relative to $\tilde{\pi}_f$, and is strictly better whenever such refinements occur
 1019 with positive probability.

1020 Now let π_f denote any soft-signal policy produced by our framework. Since π_f can always ignore
 1021 the extra information and implement $\tilde{\pi}_f$, we have

$$1022 \quad \mathbb{E}_\theta \mathbb{E}_{x_T \sim \pi_f(\cdot | \theta)}[R^0(x_T, \theta)] \geq \mathbb{E}_\theta \mathbb{E}_{x_T \sim \tilde{\pi}_f(\cdot | \theta)}[R^0(x_T, \theta)]. \quad (*)$$

1023 The case $T = 1$ (zero-shot) follows verbatim by replacing x_T with the single-step x . \square

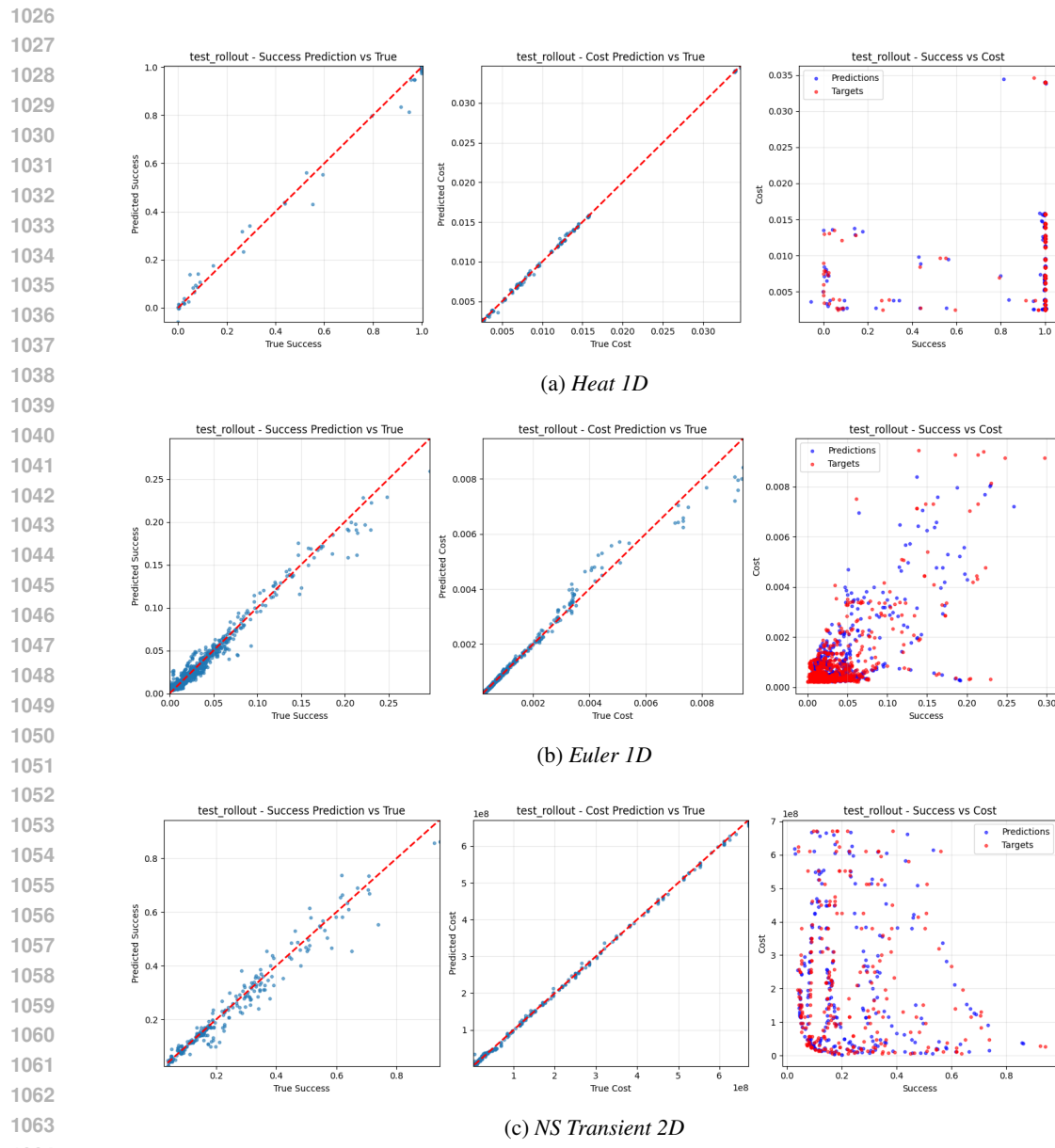


Figure 8: Test results of our best neural network for each task. The plots from left to right respectively mean: (left) soft utility signal of true RMSE loss vs. soft utility signal of predicted RMSE loss, (middle) true cost vs. predicted cost, (right) distribution in the cost-utility space of predicted vs. true points.

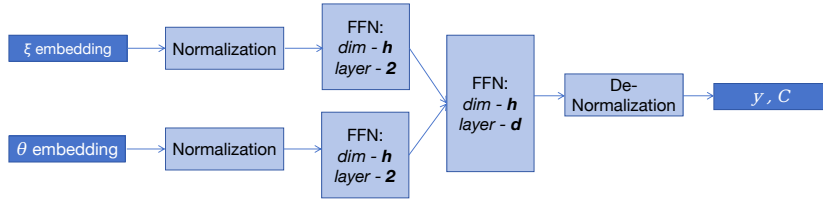


Figure 9: Neural-Network Structure

1080
1081

In this work, we define the soft utility function $f(r)$ as follows:

1082
1083
1084
1085

$$f(r) = \begin{cases} 1.0 & \text{if } d \leq \epsilon \\ \alpha e^{-\beta(r-1)^\gamma} + (1 - \alpha) \left(\frac{1}{1+\omega(r-1)^\delta} \right) & \text{if } d > \epsilon, \end{cases} \quad (10)$$

1086
1087

where $r = \frac{d}{\epsilon}$. The parameters are set to $\alpha = 0.6$, $\beta = 0.43$, $\gamma = 1.5$, $\omega = 0.3$, and $\delta = 2.2$.

1088
1089
1090

This function is designed so that the utility value drops to approximately 0.5 when the distance d is double the tolerance ϵ (i.e., $r = 2$), and it decays rapidly towards zero as the distance increases further, becoming negligible for distances approaching 10ϵ (i.e., $r = 10$). A plot of $f(r)$ is shown in Figure 10.

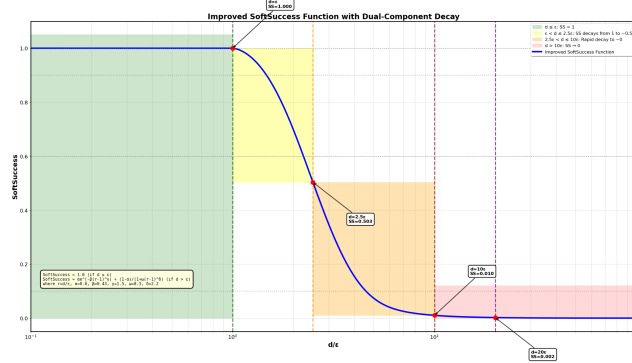
1091
1092
1093
1094
1095
1096
1097
1098
1099
1100
1101
11021103
1104
1105

Figure 10: Plot of the soft utility function $f(r)$. The function maintains a maximum utility of 1.0 for normalized distances $r \leq 1$, drops to approximately 0.5 at $r = 2$, and rapidly decays towards zero for larger values of r .

1106

E PROMPTS USED IN AGENT FRAMEWORK

1109

Prompt Example for Euler 1D Single-Turn w/ Scenario Setting

1110

Instruction

1111
1112
1113
1114
1115
1116

Your task is to find the optimal parameter, solving the 1D Euler equations for compressible inviscid flow, using a 2nd order MUSCL scheme with Roe flux and generalized superbee limiter. This serves as a simplified model for compressible fluid dynamics. You should try to minimize the total cost incurred by function calls, but your primary goal is to successfully meet the convergence criteria. You should always use the tool call function to finish the problem.

1117
1118
1119
1120
1121
1122

Workflow: n_space (Number of grid cells) determines the spatial discretization resolution: $\Delta x = L/n_space$ where L is the domain length. You may **only** change ‘n_space’. The value of k is **-1.0**, beta is **1.0**, cfl is **0.25**. **You must not change them!** You have only one opportunity to choose an optimal value for n_space. No trial-and-error or iterative optimization is permitted. Your goal is to select a value that provides adequate spatial resolution while keeping computational cost reasonable.

1123
1124
1125

Step 1: Make your best **one-shot** guess for n_space.

Step 2: Call the Convergence Test Function and check if converged.

Step 3: Output final answer with no further tool calls.

1126

Input

1127

QID: 1

1128

Problem: Euler 1D Equations with 2nd Order MUSCL-Roe Method

1129
1130
1131

This simulation solves the 1D Euler equations for compressible inviscid flow, using a 2nd order MUSCL scheme with Roe flux and generalized superbee limiter:
Conservative form:

1132
1133

$$\frac{\partial \mathbf{U}}{\partial t} + \frac{\partial \mathbf{F}(\mathbf{U})}{\partial x} = 0$$

1134 Where the conservative variables and flux are:
 1135
 1136 $\mathbf{U} = \begin{pmatrix} \rho \\ \rho u \\ \rho E \end{pmatrix}, \quad \mathbf{F} = \begin{pmatrix} \rho u \\ \rho u^2 + p \\ u(\rho E + p) \end{pmatrix}$
 1137
 1138
 1139 Primitive variables:
 1140

- ρ = density
- u = velocity
- p = pressure
- E = specific total energy

 1141 Equation of state:
 1142
$$p = (\gamma - 1)\rho \left(E - \frac{u^2}{2} \right)$$

 1143 where γ is the ratio of specific heats.
 1144 Spatial Discretization: The spatial discretization uses MUSCL reconstruction with blending
 1145 parameter k :
 1146
 1147
$$\mathbf{U}_{j+\frac{1}{2}}^L = \mathbf{U}_j + \frac{1+k}{4} \psi(r_j)(\mathbf{U}_{j+1} - \mathbf{U}_j)$$

 1148
 1149
$$\mathbf{U}_{j+\frac{1}{2}}^R = \mathbf{U}_{j+1} - \frac{1+k}{4} \psi(r_{j+1})(\mathbf{U}_{j+2} - \mathbf{U}_{j+1})$$

 1150 where k is a blending coefficient between central ($k = 1$) and upwind ($k = -1$) scheme, and
 1151 $\psi(r)$ is the slope limiter function.
 1152 Slope Limiting: The slope limiter uses a generalized superbee limiter:
 1153
 1154
$$\psi(r) = \max [0, \max [\min(\beta r, 1), \min(r, \beta)]]$$

 1155 where β is the limiter parameter controlling dissipation.
 1156 The slope ratio r at interface j is defined as:
 1157
 1158
$$r_j = \frac{\mathbf{U}_{j+1} - \mathbf{U}_j}{\mathbf{U}_{j+2} - \mathbf{U}_{j+1}}$$

 1159 This ratio indicates the local non-smoothness, which will be the input into the slope limiter to
 1160 achieve the TVD condition.
 1161 Flux Computation: The interface flux is computed using the Roe approximate Riemann solver:
 1162
 1163
$$\mathbf{F}_{j+\frac{1}{2}} = \frac{1}{2} [\mathbf{F}(\mathbf{U}^L) + \mathbf{F}(\mathbf{U}^R)] - \frac{1}{2} |\mathbf{A}| (\mathbf{U}^R - \mathbf{U}^L)$$

 1164 where $|\mathbf{A}|$ is the Roe matrix with Roe-averaged quantities.
 1165 Initial condition cases:
 1166

- sod: Left: $\rho = 1.0, u = 0.0, p = 1.0$; Right: $\rho = 0.125, u = 0.0, p = 0.1$
- lax: Left: $\rho = 0.445, u = 0.6977, p = 3.528$; Right: $\rho = 0.5, u = 0.0, p = 0.571$
- mach_3: Left: $\rho = 3.857, u = 0.92, p = 10.333$; Right: $\rho = 1.0, u = 3.55, p = 1.0$

 1167 Parameter Information:
 1168

- cfl: Courant-Friedrichs-Lowy number, $CFL = \frac{(|u|+c)\Delta t}{\Delta x}$ where $c = \sqrt{\gamma p / \rho}$ is the speed of sound
- beta: Limiter parameter for generalized superbee
- k: Blending parameter between central and upwind fluxes
- n_space: Number of grid cells for spatial discretization, determines spatial resolution: $\Delta x = L/n_space$

 1169 Physical Parameters:
 1170

- Domain length: 1.0

1188 • Gamma (ratio of specific heats): 1.4
 1189 • Case: sod

1190 Convergence Check:
 1191 • Errors between the simulation based on your solution and the simulation based on the self-refined solution are computed to assess convergence.
 1192 • Convergence is confirmed if the following validation criteria are satisfied.

1193 Validation Criteria:
 1194 • **Current Problem Precision Level:** HIGH
 1195 • **Required RMSE Tolerance:** ≤ 0.01
 1196 • Relative RMSE must meet this tolerance compared to self-refined solution
 1197 • Positivity preservation: pressure and density must remain positive at all times
 1198 • Shock speed consistency: pressure gradients should not exceed physical bounds

1199 **Available functions:**

1200 Function Name: euler_1d_check_converge_n_space
 1201 Description: Conduct a 1D Euler PDE simulation and evaluate its spatial convergence by doubling n_space. It returns the following results:

1202 • RMSE: float
 1203 • is_converged: boolean
 1204 • accumulated_cost: integer
 1205 • The cost of the solver simulating the environment: integer
 1206 • The cost of the solver verifying convergence (This will not be included in your accumulated_cost): integer
 1207 • metrics1: object
 1208 • metrics2: object

1209 Parameters:
 1210 • cfl (float): CFL number
 1211 • beta (float): Limiter parameter for generalized superbee
 1212 • k (float): Blending parameter for MUSCL reconstruction
 1213 • n_space (integer): Current number of grid cells for spatial discretization

1214 Required parameters: cfl, beta, k, n_space **Design-Value History**

1215 Below are some previous n_space values and their simulation accuracy
 1216 and efficiency indicators. The values are arranged in ascending
 1217 order based on accuracy, where higher values indicate a closer
 1218 simulation result to ground truth. The efficiency indicator is
 1219 also important, where higher values mean a more cost-efficient
 1220 n_space choice.

1221 <n_space> 240 </n_space>
 1222 Accuracy Indicator:
 1223 0.9834
 1224 Efficiency Indicator:
 1225 1.1479

1226 <n_space> 512 </n_space>
 1227 Accuracy Indicator:
 1228 1.0000
 1229 Efficiency Indicator:
 1230 0.2717

```

1242
1243 <n_space> 400 </n_space>
1244   Accuracy Indicator:
1245   1.0000
1246   Efficiency Indicator:
1247   0.4255
1248
1249 <n_space> 300 </n_space>
1250   Accuracy Indicator:
1251   1.0000
1252   Efficiency Indicator:
1253   0.7290
1254
1255 <n_space> 288 </n_space>
1256   Accuracy Indicator:
1257   1.0000
1258   Efficiency Indicator:
1259   0.7897
1260
1261 <n_space> 260 </n_space>
1262   Accuracy Indicator:
1263   1.0000
1264   Efficiency Indicator:
1265   0.9707
1266
1267 <n_space> 258 </n_space>
1268   Accuracy Indicator:
1269   1.0000
1270   Efficiency Indicator:
1271   0.9865
1272
1273 <n_space> 257 </n_space>
1274   Accuracy Indicator:
1275   1.0000
1276   Efficiency Indicator:
1277   0.9946
1278
1279 <n_space> 256 </n_space>
1280   Accuracy Indicator:
1281   1.0000
1282   Efficiency Indicator:
1283   1.0027
1284
1285 <n_space> 252 </n_space>
1286   Accuracy Indicator:
1287   1.0000
1288   Efficiency Indicator:
1289   1.0364
1290
1291 Output final answer in the requested format with a new n_space value
1292 ↳ that is different from all values above. You should first ensure
1293 ↳ an accurate simulation by achieving 1.0 in accuracy indicator,
1294 ↳ then gradually increase efficiency by choosing a coarser n_space
1295 ↳ value.

```

Prompt Example for Euler 1D Single-Turn w/. Scenario Setting

Instruction

Your task is to optimize a one-dimensional black-box function with a given parameter. You will be prompted with a list of history of parameter and values, where values include an accuracy indicator and success indicator. You are required to first optimize accuracy until it reaches

1296
 1297 1.0, then optimize efficiency for as high as possible. The parameter in history will start with
 1298 <n_space> and end with </n_space>. Please return a parameter value different from all values
 1299 given in the history that you think will optimize the function value as requested. Please return
 1300 your answer by starting with <n_space> and ending with </task> as well. **You may NOT use**
 1301 **any form of prior knowledge, and treat all parameter names, function names, etc. as**
 1302 **purely arbitrary.**

1303 **Input**

1304 **Design-Value History**

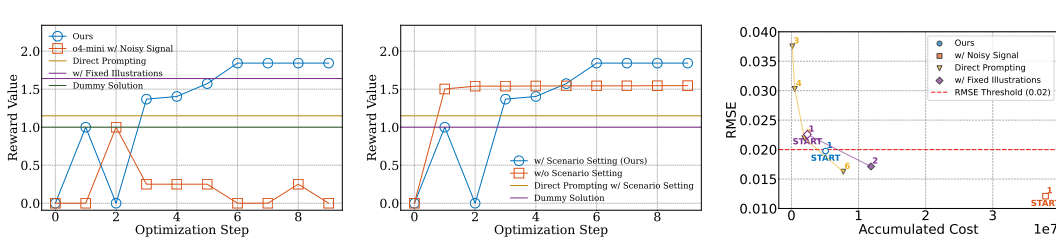
1305
 1306 Below are some previous n_space values and their simulation accuracy
 1307 → and efficiency indicators. The values are arranged in ascending
 1308 → order based on accuracy, where higher values indicate a closer
 1309 → simulation result to ground truth. The efficiency indicator is
 1310 → also important, where higher values mean a more cost-efficient
 1311 → n_space choice.

1312 <n_space> 240 </n_space>
 1313 Accuracy Indicator:
 1314 0.9834
 1315 Efficiency Indicator:
 1316 1.1479
 1317
 1318 <n_space> 512 </n_space>
 1319 Accuracy Indicator:
 1320 1.0000
 1321 Efficiency Indicator:
 0.2717
 1322
 1323 <n_space> 400 </n_space>
 1324 Accuracy Indicator:
 1325 1.0000
 1326 Efficiency Indicator:
 0.4255
 1327
 1328 <n_space> 300 </n_space>
 1329 Accuracy Indicator:
 1330 1.0000
 1331 Efficiency Indicator:
 0.7290
 1332
 1333 <n_space> 288 </n_space>
 1334 Accuracy Indicator:
 1335 1.0000
 1336 Efficiency Indicator:
 0.7897
 1337
 1338 <n_space> 260 </n_space>
 1339 Accuracy Indicator:
 1340 1.0000
 1341 Efficiency Indicator:
 0.9707
 1342
 1343 <n_space> 258 </n_space>
 1344 Accuracy Indicator:
 1345 1.0000
 1346 Efficiency Indicator:
 0.9865
 1347
 1348 <n_space> 257 </n_space>
 1349 Accuracy Indicator:

```

1350
1351     Efficiency Indicator:
1352     0.9946
1353
1354     <n_space> 256 </n_space>
1355     Accuracy Indicator:
1356     1.0000
1357     Efficiency Indicator:
1358     1.0027
1359
1360     <n_space> 252 </n_space>
1361     Accuracy Indicator:
1362     1.0000
1363     Efficiency Indicator:
1364     1.0364
1365
1366     Output final answer in the requested format with a new n_space value
1367     ↳ that is different from all values above. You should first ensure
1368     ↳ an accurate simulation by achieving 1.0 in accuracy indicator,
1369     ↳ then gradually increase efficiency by choosing a coarser n_space
1370     ↳ value.
1371
1372
1373 F DETAILED RESULTS
1374
1375
1376
1377
1378
1379

```



(a) An exemplar optimization trajectory in Single-Turn setting for CAED-Agent with vs. without scenario setting.

Figure 11: Case studies for ablations, with base model OpenAI o4-mini.

Full results of the comprehensive benchmark are presented in table 2. The case studies as introduced in 4.5 are shown in Figure 11.

The full ablation results are presented in table 3. Our ablations on surrogate neural network and prior knowledge are conducted on *Euler 1D*'s medium precision level tasks; we report reward R^0, R^m and success rates P^0, P^m for both Single-Turn and Multi-Turn settings. Our base model is fixed as o4-mini. Note that although CAED-Agent without Physics prior is achieving a higher mean reward in Single-Turn setting, its success rate is much lower than our method, indicating its frequent choice of coarse designs that leads to high reward in only a few tasks. We argue that this is a form of reward hacking as it contradicts with our expectation to carry out experiments correctly and efficiently.

```

1394
1395
1396
1397
1398
1399
1400
1401
1402
1403

```

Table 2: Main evaluation results in both Single-Turn and Multi-Turn settings. Values in each box is the mean of tasks evaluated in three precision levels. Note that we report both reward R^0 , R^m and for-reference quantities P^0 and P^m . Values in bold font are the best-achieving ones, and values with \uparrow indicate a significant rise compared to direct prompting.

(a) Single-Turn CAED-Agent

Method	Base Model	Heat ID		Euler ID		NS Transient 2D	
		R^0	P^0	R^0	P^0	R^0	P^0
BO (Nogueira, 2014)	–	0.253	1.000	0.464	0.125	0.814	0.718
Base LLM	Llama3.2-3B-Instruct	0.288	0.347	0.698	0.174	0.052	0.151
	Qwen-8B	0.412	0.633	0.642	0.268	0.342	1.000
	o4-mini	0.362	0.253	0.501	0.301	0.565	0.516
<i>CAED-Agent</i> (Ours)	Llama3.2-3B-Instruct	0.950 \uparrow	0.773 \uparrow	0.939 \uparrow	0.516 \uparrow	1.591 \uparrow	0.785 \uparrow
	Qwen-8B	0.853 \uparrow	0.759 \uparrow	0.897 \uparrow	0.789 \uparrow	1.813 \uparrow	0.702
	o4-mini	1.239 \uparrow	0.679 \uparrow	1.764 \uparrow	0.733 \uparrow	0.842 \uparrow	0.536

(b) Multi-Turn CAED-Agent

Method	Base Model	Heat ID		Euler ID		NS Transient 2D	
		R^m	P^m	R^m	P^m	R^m	P^m
BO (Nogueira, 2014)	–	0.290	1.000	0.496	0.625	0.517	0.766
Base LLM	Llama3.2-3B-Instruct	1.060	0.837	0.328	0.531	1.232	0.448
	Qwen-8B	1.613	0.756	1.511	0.421	0.662	0.861
	o4-mini	1.960	0.960	1.135	0.392	0.991	0.674
OPRO (Yang et al., 2023)	Llama3.2-3B-Instruct	0.170	0.917	0.290	0.600	0.275	0.877
	Qwen-8B	0.217	0.917	0.323	0.680	0.326	1.000
	o4-mini	0.241	0.917	0.974	0.520	0.957	1.000
<i>CAED-Agent</i> (Ours)	Llama3.2-3B-Instruct	1.204 \uparrow	0.946 \uparrow	1.339 \uparrow	0.572	1.435	0.925 \uparrow
	Qwen-8B	1.760	0.900 \uparrow	1.359	0.624 \uparrow	1.535 \uparrow	0.944
	o4-mini	1.981	0.986	1.571 \uparrow	0.443	1.538 \uparrow	0.972 \uparrow

Table 3: Ablation results averaged over all tasks.

Setting	Single-Turn Setting		Multi-Turn Setting	
	R^0	P^0	R^m	P^m
<i>CAED-Agent</i> (Ours)	0.571	0.708	0.834	1
<i>CAED-Agent</i> w/ Sparse Surrogate Signal	0.42	0.5	0.635	0.875
<i>CAED-Agent</i> w/ Random Signal	0.142	0.583	0.426	0.583
<i>CAED-Agent</i> w/ In-Context Signal	0.42	0.5	0.572	0.958
<i>CAED-Agent</i> w/o Physics Prior	0.595	0.152	0.475	0.375
Direct Prompting	0.096	0.125	0.116	0.167